ELSEVIER

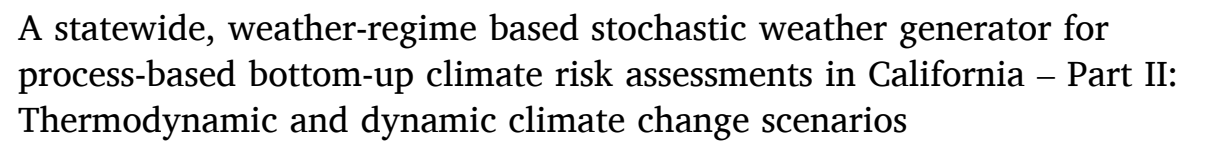
Contents lists available at ScienceDirect

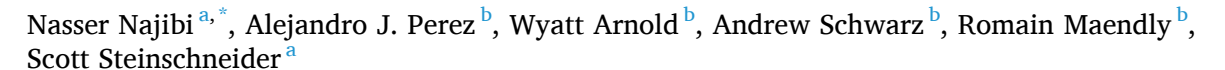
Climate Services

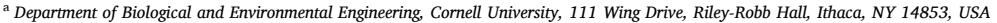
journal homepage: www.elsevier.com/locate/cliser



Original research article







^b California Department of Water Resources, 715 P Street, Sacramento, CA 95814, USA

HIGHLIGHTS

- A weather regime-based stochastic weather generator is utilized to create thermodynamic and dynamic climate change scenarios.
- The ensemble comprises 32, 1000-yr climate scenarios for changes in temperature, precipitation, and atmospheric circulation.
- The scenarios are intended to support bottom-up climate vulnerability assessments of water systems across California.

ARTICLE INFO

Keywords: Climate change Thermodynamic change Dynamic change Decision-making Bottom-up Water resources California

ABSTRACT

This study is the second of a two-part series presenting a novel weather regime-based stochastic weather generator to support bottom-up climate vulnerability assessments of water systems in California. In Part 2 of this series, we present how the model is used to develop an ensemble of climate change scenarios based on both thermodynamic and dynamic signals of climate change. The ensemble includes a suite of 30 climate change scenarios, each consisting of 1000 years of simulated daily climate data (precipitation, maximum temperature, minimum temperature) at a 6 km resolution across the entire state of California. The 30 scenarios represent a range of plausible climate changes to temperature, average precipitation, and precipitation extremes that are reflective of thermodynamic responses of the atmosphere to warming. An additional two scenarios are also created that represent changes in the frequency of weather regimes (e.g., dynamic climate change). Results from these scenarios reveal that when the effects of anthropogenic climate change are combined with plausible realizations of natural climate variability, the severity of extremes in California is amplified significantly. In addition, recent changes in the frequency of large-scale patterns of atmospheric circulation can have impacts of similar magnitude to large (>10%) declines in average precipitation, particularly with respect to drought. The scenarios developed in this work are designed to allow water managers to systematically test the sensitivity of their water system to different combinations of climate change, so that key vulnerabilities can be discovered and then addressed through adaptation planning.

Practical implications

Water resource planners in California must prepare for the increased stress of climate change. However, there is significant uncertainty about how the climate will evolve over the coming decades. While most climate projections agree that California's future will be warmer and precipitation will intensify, the rate of

these changes is less clear, as are more nuanced climate changes like shifts in average precipitation or changes to atmospheric circulation that can impact regional weather. Furthermore, water systems in California are very vulnerable to natural swings in climate unrelated to climate change, and the range of this natural variability must also be considered in future planning efforts.

This two-part series comprises a pair of articles documenting the

^{*} Corresponding author at: 111 Wing Dr, Riley-Robb Hall 325, Ithaca 14853, NY, USA. *E-mail address*: nn289@cornell.edu (N. Najibi).

development of a stochastic weather generator for California that can create large ensembles of climate traces to support water resources planning under future climate uncertainty. The weather generator is an efficient tool that can quickly create long (1000-year) traces of statewide weather, and allows water managers to flexibly develop and explore climate scenarios associated with different signals of climate change. These include 'thermodynamic' changes (i.e., more intense precipitation linked to an increase in the moisture-holding capacity of warmer air), as well as more nuanced signals related to shifts in atmospheric circulation (i.e., dynamic climate change).

In Part (1) of this series, we presented the development and validation of the model. In this article (i.e., Part (2) of the series), we focus on the development of climate change scenarios. The work in Part (2) details the creation of a publicly available dataset of 30 unique climate change scenarios, each consisting of 1000 years of simulated climate data (precipitation, maximum temperature, minimum temperature) at a 6 km resolution across the entire state of California. The 30 scenarios represent a range of plausible climate changes to temperature, average precipitation, and precipitation extremes. These include five scenarios of temperature change ranging from 1 °C to 5 °C of warming at 1 °C increments and five scenarios of mean precipitation change ranging from -25% to +25% of historical averages at 12.5% increments. For all twenty-five of these scenarios, we scale extreme daily precipitation with temperature at a rate of 7% per °C of warming, to reflect the increased moisture holding capacity of the atmosphere according to the Clausius-Clapeyron relationship. We generate four additional climate change scenarios that use different scaling rates (0% per °C and 14% per °C of warming) to support sensitivity analysis with respect to extreme precipitation scaling. Together with the baseline scenario containing no climate change, this leads to 30 scenarios altogether, which form the primary data product from this study. We also create two experimental climate scenarios that reflect changes to the frequency of large-scale weather patterns, based on a preliminary analysis of historical trends in these patterns. However, these experimental scenarios are not included in the data release associated with this work.

The datasets created in this work highlight how even in the absence of climate change, water managers in California should plan for extreme precipitation events and droughts beyond the worst case from the historical record, because such events are quite plausible due to California's natural climate variability alone. However, when such natural extremes are combined with the effects of anthropogenic climate change, extremes in California become severe and will likely require significant investment in water resources systems to sustain adequate water services across the state. The weather generator and associated datasets should be viewed as a complementary tool to more commonly available downscaled GCM projections. Unlike GCMs, the weather generator is not designed to create scenarios of future climate based on the physical laws of the Earth system and future greenhouse gas emission scenarios. Rather, the model provides a way to help translate various signals of climate change from GCMs into traces of weather that are tailored to support water resource planning efforts. In this way, the California weather generator is envisioned as a tool to help promote collaboration between climate scientists and water resource planners across the state.

Stakeholders across California can utilize the climate scenarios produced by the stochastic weather generator to infer the joint impact of both climate change and natural climate variability on their systems. We recommend that stakeholders use the data products developed in this work in stages to help develop robust adaptations of water resources infrastructure under climate change. For example, initial adaptation strategies (e.g., new reservoir operational policies, new infrastructure for managed aquifer recharge) could be developed using the historical record to ensure these strategies are able to meet performance requirements under past and recent extreme events. Then, these strategies could be re-evaluated using: 1) a 1000-year baseline weather generator simulation; and 2) climate change scenarios applied to the 1000-

year weather generator simulation. These evaluations would provide information on how robust a given adaptation strategy is to natural climate variability, climate change, and a combination of the two.

Such information could be used in different ways to alter the initial adaptation strategy. For instance, if a strategy appears vulnerable to the 1000-year baseline weather generator simulation (i.e., natural climate variability) or scenarios from the model reflective of likely future climate conditions (e.g., a low degree of future warming projected in most GCMs over the next few decades), this might suggest an immediate need for a more robust strategy. Alternatively, in cases where an adaptation strategy is only vulnerable to the most extreme climate change scenarios produced by the model, the current adaptation strategy may be deemed adequate if coupled with plans for continued climate monitoring and retrofits/adjustments that could be implemented later if needed.

1. Introduction

Climate change presents a major concern for water security at local, regional, and global scales (Ranasinghe et al., 2021; IPCC, 2022). In California, climate change experienced to date has already exacerbated recent droughts via warming temperatures and enhanced drying power of the atmosphere (Williams et al., 2022). Similarly, extreme precipitation during recent, atmospheric river (AR)-related storms was likely more intense than it otherwise would have been due to warming temperatures and an associated increase in the moisture holding capacity of the atmosphere following the Clausius-Clapeyron relationship (Gonzales et al., 2019; Michaelis et al., 2022). These climate changes are related to thermodynamic responses of the atmosphere to a warmer climate, and global climate models (GCMs) project that these types of thermodynamic climate change will accelerate over California and much of the U. S. Southwest into the middle and end of the 21st century (Espinoza et al., 2018; Massoud et al., 2019; Rhoades et al., 2020; Overpeck and Udall, 2020; Huang and Swain, 2022). Other first-order responses to surface warming include greater frequency of extreme heat (Ullrich et al., 2018) and significant changes to seasonal snow accumulation and melt patterns (Berg and Hall, 2017; Ishida et al., 2019; He et al., 2021; Shulgina et al., 2023). Generally, projections of thermodynamic climate changes are consistent across theory, observations, and model projections (Pfahl et al., 2017; Allan et al., 2020), leading to high confidence in the direction of future change, although with residual uncertainty in the ultimate rate of change.

Other types of long-term climate changes are also possible, but with a greater degree of uncertainty (Shepherd, 2014; Elbaum et al., 2022). For instance, shifts in atmospheric circulation, or dynamic climate changes, have been observed and projected for California. Zhang et al. (2022) recently showed a 40-year decline (from 1980 to 2018) in the frequency of a deep trough over Western North America that is associated with strong moisture flux and precipitation in California. This trend in the frequency of one large-scale atmospheric flow pattern appears to explain much of the drying trend observed over California and the Southwestern U.S. during that same period, and an ensemble of historical CMIP6 climate model simulations suggest these observed shifts in atmospheric circulation have been driven by anthropogenically forced climate change. Others have also explored how late 21st century projections of these atmospheric flow patterns influence future climate over the Western U.S. For instance, Swain et al. (2018) found that changes in the spatial pattern and intensity of atmospheric circulation patterns may be responsible for projected increases in the frequency of dry and wet regimes in California. Shields and Kiehl (2016) focused specifically on the landfall locations of ARs along the West Coast and projected that landfalling ARs will eventually move equatorward during winter. However, others (Gao et al., 2016; Ma et al., 2020) have identified an opposite,

poleward movement of ARs in other regions of the world, highlighting that there is substantial regional variability and uncertainty in this type of dynamic climate change for ARs (Payne et al., 2020).

In Part (1) of this two-part series, we introduced and validated a weather regime-based stochastic weather generator designed to support bottom-up climate vulnerability assessments of water systems. Vulnerability assessments seek to define the range of climate conditions that lead to critical system vulnerabilities (see Fig. 1), and therefore are most relevant to the decision-making process of climate adaptation (Brown et al., 2012). Such frameworks help circumvent the issue of severe uncertainty in more traditional top-down climate impact assessments, in which downscaled GCM projections are used to drive the entire analysis. Bottom-up vulnerability assessments ensure a thorough exploration of system sensitivities to small perturbations in climate that might not be captured when using a relatively small and often biased GCM ensemble. However, these assessments can still use GCM-based information to help define the range of plausible future climate changes and their likelihood. Key to these vulnerability assessments is the ability to generate long climate traces useful for quantifying both water supply and flood risk, and to do so for many scenarios of potential climate change selected according to a carefully crafted experimental design (Steinschneider et al., 2015; Schwarz et al., 2018; CA DWR, 2019; Ray et al., 2020). Stochastic weather generators provide exactly this functionality.

In the present study (Part 2 of this two-part series), we detail how the stochastic weather generator described in Part (1) can be used to produce an ensemble of thermodynamic and dynamic climate change scenarios to support bottom-up climate impact assessments of water systems across the state of California. We review the weather generator and describe how it is used to produce these scenarios in Section 2. In Section 3, we present these future climate scenarios and their impacts on different metrics of average and extreme precipitation and temperature. We conclude in Section 4 with a discussion of model limitations and guidance for use of these data products.

2. Methods

2.1. Overview of stochastic weather generator

In this work, we use the stochastic weather generator described in Part (1) of this series to generate an ensemble of future climate scenarios

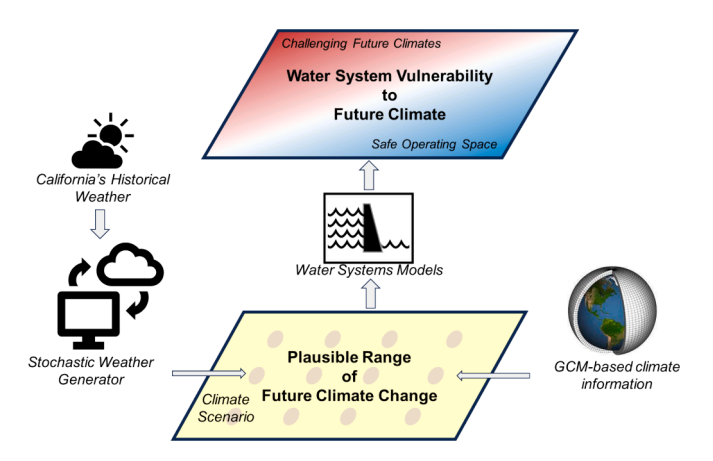


Fig. 1. Overview of bottom-up vulnerability assessments for water systems under climate uncertainty. A stochastic weather generator like the model developed in this work can be fit to California's historical weather and then used to generate a large ensemble of future climate scenarios that systematically explore a range of plausible climate changes. This range can be informed by state-of-the-art global climate model (GCM)-based information. The climate scenarios can be used as forcing for models of hydrologic and water infrastructure systems to develop a clear picture of water system vulnerabilities to different types of climate change.

across the entire state of California. The full model is described in detail in Part (1). Here, we only provide a brief overview of the model for context that supports the description of climate scenario development below. The California weather generator can be used with many different continuous climate datasets, but in this work the model uses gridded (~6 km) daily precipitation between January 1, 1948 and December 31, 2018 across California from the extreme-preserving gridded daily dataset developed by Pierce et al. (2021). Gridded, daily minimum and maximum temperature at the same resolution and for the same domain are taken from Livneh et al. (2013) for the period between January 1, 1948 and December 31, 2015, and are then extended to December 31, 2018 using the PRISM daily dataset (PRISM Climate Group, 2014). These temperature data are detrended to ensure all temperature data reflect average temperatures experienced over the last 30 years (1991–2020).

The weather generator is a semiparametric, multivariate, and multisite model that is designed to separately model dynamic and thermodynamic atmospheric mechanisms of climate variability and change through statistical abstractions of these processes. To capture atmospheric dynamics, the weather generator simulates sequences of weather regimes (WRs), which are recurring large-scale atmospheric flow patterns (e.g., upper-level, quasi-stationary blocks and troughs) that organize high-frequency weather systems (Robertson and Ghil, 1999; Robertson et al., 2015). They represent intermediary phenomena that help link slowly varying global climate circulation with weather experienced at the local scale. To capture thermodynamic mechanisms of climate change, the weather generator post-processes simulated precipitation and temperature data to reflect patterns of warming and thermodynamic scaling of precipitation rates with that warming.

These properties of the model are represented in a hierarchical structure composed of three primary modules. In the first module, a nonhomogenous Hidden Markov Model (NHMM) is used to identify and simulate WRs based on geopotential height data across the Pacific-North American sector. In the second module, 6 km gridded precipitation and maximum and minimum temperature across California are simulated through bootstrapping conditioned on the simulated WRs. Noise is added to resampled heavy precipitation events using an approach that leverages a mixture of gamma and Generalized Pareto distributions (gamma-GPD) fit to the non-zero precipitation at each gridded location. In the third module, perturbations to the simulation schemes in the first two modules are applied to impose thermodynamic and dynamic climate changes to the simulated data. The first two of these modules were described in detail in Part (1), while in Section 2.2 below we focus on the scenarios developed in the third module. Where necessary, mathematical details related to the creation of these climate scenarios are presented in Appendix A.

2.2. Thermodynamic and dynamic climate change scenarios

Most of the scenarios developed in this work focus on perturbations to climate consisting of various levels of warming and changes to the daily precipitation distribution. The number and range of scenarios across different variables were developed in collaboration with partners in the California Department of Water Resources, and were selected to reflect the range of uncertainty in different types of climate change while also acknowledging the desire of water resource practitioners to maintain a manageable number of scenarios in their planning studies.

We use the weather generator to create five different scenarios of temperature change, from +1 °C to +5 °C by 1 °C increments (see Fig. 2; Table 1). Temperature change is treated simply by adding step changes to simulated daily maximum and minimum temperature data (which have already been detrended to reflect recent warming) uniformly across the entire spatial domain. This range of temperature increase was inferred from an ensemble of climate model projections selected by the California Department of Water Resources Climate Change Technical Advisory Group (CA-DWR CCTAG, 2015). Those projections, taken from

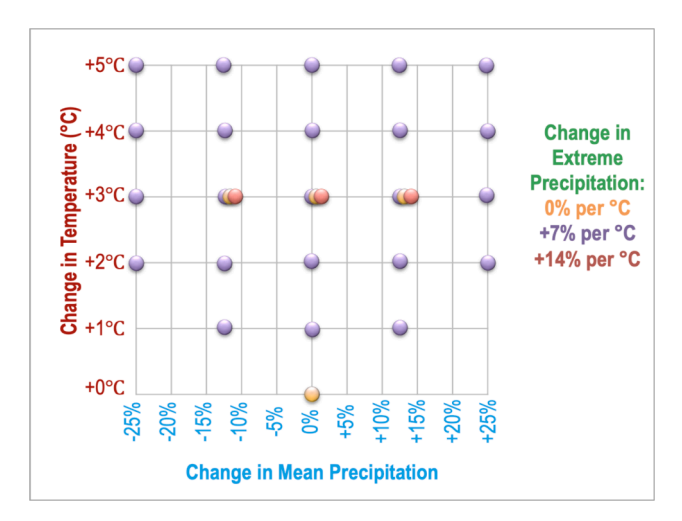


Fig. 2. Range of climate change scenarios developed under this work.

Table 1
List of 30 climate scenarios

Scenario Number	Incremental Temperature Change [°C]	% Change Extreme Precipitation Quantile	% Change Precipitation Mean
1: baseline	0	0	0
2	2	7	-25
3	3	7	-25
4	4	7	-25
5	5	7	-25
6	1	7	-12.5
7	2	7	-12.5
8	3	7	-12.5
9	4	7	-12.5
10	5	7	-12.5
11	1	7	0
12	2	7	0
13	3	7	0
14	4	7	0
15	5	7	0
16	1	7	12.5
17	2	7	12.5
18	3	7	12.5
19	4	7	12.5
20	5	7	12.5
21	2	7	25
22	3	7	25
23	4	7	25
24	5	7	25
25	3	0	-12.5
26	3	0	0
27	3	0	12.5
28	3	14	-12.5
29	3	14	0
30	3	14	12.5

a subset of ten high-performing GCMs for California from the CMIP5 archive, suggested that $+5\,^{\circ}\text{C}$ was approximately the maximum amount of warming that could be expected towards the end of the 21st century under the RCP 8.5 emission scenario, based on a multi-model average.

Scenarios of precipitation intensification are modeled by scaling the distribution of daily precipitation in a way that replicates the thermodynamic effects of warming temperatures on precipitation through increases in the moisture holding capacity of the atmosphere. In California, past work has shown that warming temperatures will lead to an increase in the most intense precipitation events (often associated with ARs) but a decline in the magnitude of smaller precipitation events (Gershunov et al., 2019). This type of change effectively stretches the daily precipitation distribution, making extreme events more extreme

and suppressing the magnitude and frequency of lighter precipitation events (see Fig. 3 for an illustration). Similar to other studies (Pendergrass and Hartmann, 2014), we mimic this effect by imposing changes to the moments and quantiles of the precipitation distribution as a function of warming. Specifically, we select a scaling rate for the 99th percentile of non-zero precipitation and adjust a gamma-GPD mixture distribution fit to each site by month (see Part 1) to impose that selected scaling rate. For instance, if we assume a scenario with 2 °C of warming and a 7% per °C increase in extreme precipitation (which would match the theoretical Clausius-Clapeyron rate of increase in atmospheric water holding capacity with warming; Najibi and Steinschneider, 2023), then the most extreme precipitation events should increase by \sim 14.4% (1.07 2). We adjust the gamma-GPD models fit to all sites to require this percent change in the far upper tail of the distribution. If mean precipitation is held constant at baseline levels, this change will force smaller precipitation values under the gamma-GPD model to decrease in order to compensate for the increases in extreme events, i.e., the distribution of non-zero precipitation will be stretched, similar to the model-based results of Gershunov et al. (2019).

Once new model parameters of the gamma-GPD model are determined for each site and month, daily simulated precipitation is adjusted by first determining the non-exceedance probability, then jittering the non-exceedance probability if the simulated value is associated with heavy precipitation (to enable previously unobserved precipitation extremes), and finally determining a new precipitation value based on the adjusted gamma-GPD distribution. This procedure is repeated for each non-zero precipitation amount for each site simulated by the weather generator. The mathematical details of this approach are presented in Appendix A.1.

We enforce a 7% per °C increase in extreme precipitation for all climate scenarios developed in this work (Fig. 2, Table 1), as this rate of extreme precipitation scaling is theoretically the best supported based on the rate at which the atmospheric moisture holding capacity increases with warming. However, as a sensitivity analysis, we also develop a subset of scenarios with 0% per °C and 14% per °C increase in extreme precipitation (only for 3 °C of warming), in order to assess how

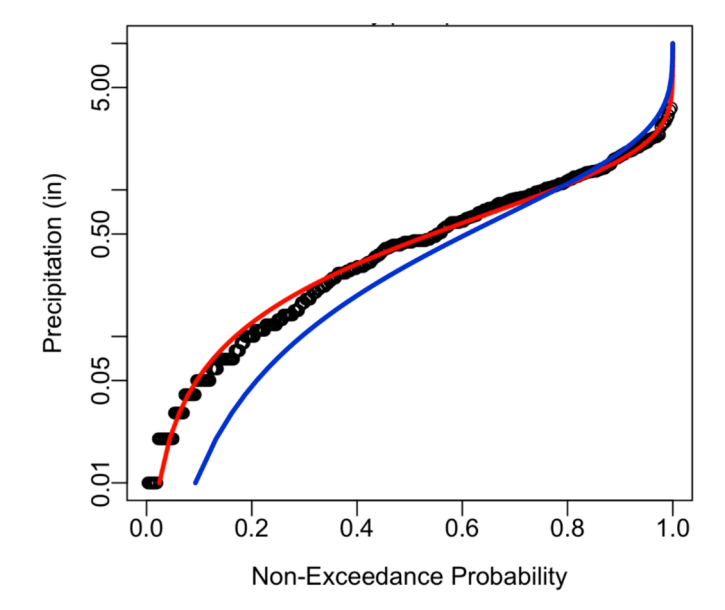


Fig. 3. Illustration of thermodynamically driven changes to the distribution of daily, non-zero precipitation. The historical distribution of precipitation (*black points* and *red line*) changes under warming such that the largest precipitation events (at high non-exceedance probabilities) become even larger (*blue line*). If average precipitation does not change under warming, then low and moderate precipitation events must scale downward to balance the increases at the upper end of the distribution. (For interpretation of the references to color in this figure legend, the reader is referred to the web version of this article.)

important extreme precipitation scaling is for water systems performance. Importantly, the degree to which extreme precipitation is scaled is directly tied to the temperature trends imposed, thus respecting the underlying thermodynamic mechanism that drives scaling. That is, precipitation scaling in the model is entirely determined after specifying a temperature trend and a scenario of precipitation scaling per degree warming.

In addition to the thermodynamic climate changes in temperature and extreme precipitation described above, we also develop scenarios of change in mean precipitation. Part of the signal around mean precipitation change may be related to the overall increase in atmospheric moisture linked to warming (a thermodynamic signal), while other components of change in mean precipitation are related to shifts in atmospheric circulation (a dynamic signal). Therefore, changes in mean precipitation reflect a mix of thermodynamic and dynamic climate changes. We consider five different scenarios of mean precipitation change, ranging from -25% to +25% of baseline levels by 12.5% increments. Similar to temperature, this range was based on a subset of end-of-21st-century CMIP5 projections selected by the CA DWR Climate Change Technical Advisory Group. We limit mean precipitation changes to $\pm 12.5\%$ for scenarios with only 1 °C of warming to acknowledge the relationship between more intense future warming and larger changes in average precipitation (see Fig. 2, Table 1). Altogether, there are 29 separate scenarios of climate change developed in this work, along with a baseline scenario with no changes imposed, leading to a total of 30

Finally, we develop two additional scenarios of pure dynamical climate change, which are composed of changes to the frequency of different WRs (i.e., shifts in atmospheric circulation). We note that changes to WRs or other modes of atmospheric circulation may result as a direct response to a warming atmosphere (e.g., due to changes in geopotential heights linked to thermal expansion), but are still considered a dynamic climate change if their impacts on surface weather manifest primarily through a change in atmospheric circulation. The direction of change for these types of climate change is very uncertain, but the risk of such change for water systems throughout the state is potentially very large. Hence, in this work we seek to develop a limited number of scenarios that reflect dynamic climate change to isolate the potential vulnerabilities that may be associated with these types of change. As a proof-of-concept, we utilize recent trends in WR frequencies over the historical record to determine which WRs have changed in frequency most significantly in the observations, and then enforce a scenario of dynamic climate change where these significant changes persist into the future. We then develop a 1000-year simulation of WRs and associated weather from the stochastic weather generator with these adjusted WR frequencies (see Appendix A.2 for the methodology of this approach), assess the impacts of this scenario on key hydrologic metrics of interest (e.g., frequency and magnitude of drought and extreme precipitation events), and compare these impacts to the impacts observed under the scenarios from Table 1. This comparison will help illustrate how the severity of impacts of dynamic climate change compares to that of thermodynamic climate change scenarios.

3. Results

In Section 3.1, we demonstrate how extremes (droughts, extreme precipitation events) vary across the 30 climate scenarios delimited in Fig. 2 and Table 1. In Section 3.2, we briefly assess how these weather generator scenarios compare against projections from a recent ensemble of GCM projections downscaled using the LOCA v.2 methodology (Pierce et al., 2023). In Section 3.3, we explore the impacts associated with two dynamic climate change scenarios in which the probabilities of individual WRs are changed based on recent trends.

3.1. Thermodynamic climate scenario impacts

To begin, we first examine the spatial distribution of impacts from a subset of the 30 scenarios in Fig. 2 and Table 1. Similar to Part (1), results are aggregated and visualized at the scale of major river basins (i.e., USGS HUC-4 unit). In Figs. 4–6 below, different climate scenarios are selected for each figure based on their relevance for different climate statistics. For example, when focusing on precipitation statistics (1-day precipitation maxima and drought; Figs. 4–5), we fix the temperature change and vary the change in mean precipitation or extreme precipitation scaling rate to see their effect on those precipitation statistics. Conversely, when focusing on temperature properties (heat waves; Fig. 6), we fix the precipitation changes and focus instead on scenarios with different levels of warming and their impact on heat wave attributes.

Fig. 4 focuses on the largest maximum 1-day precipitation event across the entire record. The far left panel in Fig. 4 shows the magnitude of the 1-day precipitation maximum across the baseline scenario (no climate change). The middle and right panels of Fig. 4 show how the largest 1-day precipitation event changes under different climate scenarios. Results in the center panel are shown for scenario #13 from Table 1, in which there is 3 °C of warming, an extreme precipitation scaling rate of 7% per °C, and 0% change in mean precipitation. Here, the increase in the 1-day precipitation maxima is largely uniform across the state, around 22.5% above baseline values. This is precisely the scaling one would expect given that $1.07^3 = 1.225$. Conversely, in the right panel of Fig. 4 there is almost no change in the 1-day precipitation maxima over baseline levels. Under this scenario (#27 in Table 1, with 3 °C of warming, no extreme precipitation scaling, and a 12.5% increase in mean precipitation), mean precipitation increases but extreme precipitation is kept at baseline levels by construction. Therefore, it is the smaller precipitation events under this scenario (rather than the largest) that are shifted upward to account for the change in the mean.

Fig. 5 shows similar results to Fig. 4 but for the worst 5-year drought on record. Here, we show baseline values in the left panel and three climate scenarios in the three rightmost panels, including scenarios #13, #8, and #18 from Table 1. Under all these scenarios, temperatures warm by 3 °C and extreme precipitation scales at a rate of 7% per °C. The only difference between the scenarios is how mean precipitation changes (0 %, -12.5%, and +12.5% of baseline values). Two insights emerge from Fig. 5. First, the largest impact on the magnitude of the worst 5-year drought is caused by the change in mean precipitation, with the magnitude of change roughly following the magnitude of change in mean precipitation (on a percentage basis). Second, we note that even under the scenario with no change in mean precipitation (scenario #13), the worst 5-year drought does become slightly worse (by \sim 5%) simply due to extreme precipitation scaling. In this scenario, light precipitation events must become even lighter to keep mean precipitation unchanged while increasing the magnitude of extreme precipitation events (i.e., the daily precipitation distribution is stretched; see Fig. 3). During droughts, there is a very high proportion of dry days and light precipitation days, and so the total precipitation during these long drought events declines because of the downward shift in light precipitation events.

Similar to Figs. 4-5 for precipitation, Fig. 6 shows the impacts of different climate scenarios on the spatial distribution of heat wave characteristics, this time focused on one HUC-4 basin (the San Joaquin) for illustration. The first row of Fig. 6 shows the average frequency of heat waves per year based on the baseline and three climate scenarios (#11, #12, and #13 from Table 1). These selected scenarios have a similar extreme precipitation scaling rate of 7% per °C and 0 % changes in mean precipitation. The only difference is how temperature (minimum, maximum) increases incrementally by 1, 2, and 3 °C. We also show the average and maximum heat wave event duration across these three scenarios in the second and third rows of Fig. 6. The results show that there is a consistent increase in the average frequency of heat waves

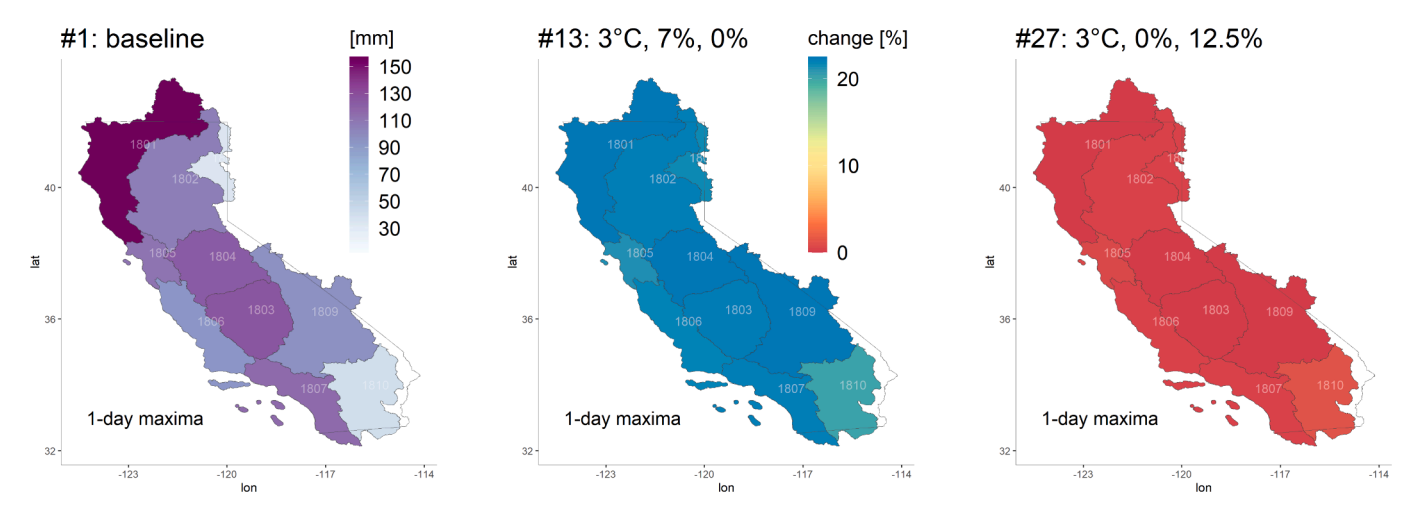


Fig. 4. (*left*) The magnitude of the largest 1-day maximum precipitation event at the HUC-4 scale in the baseline scenario (no climate change). (*middle*) The percent change in the largest 1-day maximum precipitation event from climate scenario #13 (see Table 1) with 3 °C of warming, an extreme precipitation scaling rate of 7 % per °C, and 0 % change in mean precipitation. (*right*) Same as middle panel, but for climate scenario #27 (see Table 1) with 3 °C of warming, an extreme precipitation scaling rate of 0 % per °C, and a 12.5 % increase in mean precipitation. Note that the color scale is identical for the middle and right panels.

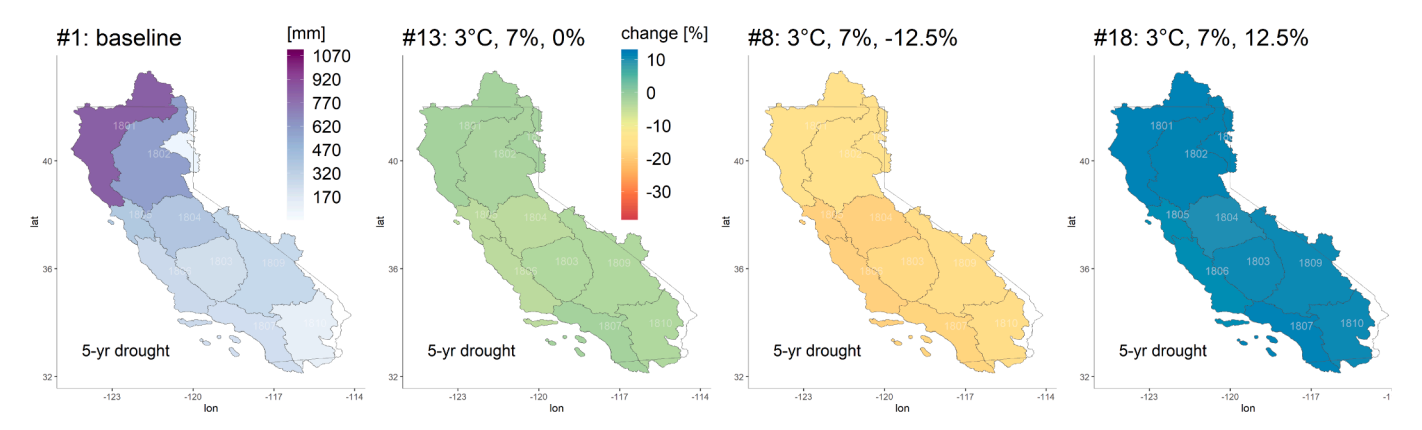


Fig. 5. (*far-left*) The magnitude of the worst 5-year drought on record at the HUC-4 scale in the baseline scenario (no climate change). (*middle-left to far-right*) The percent change in the worst 5-year drought for three climate scenarios from Table 1, including scenarios #13, #8, and #18. In all cases, temperatures warm by 3 °C and extreme precipitation scales at a rate of 7 % per °C. However, scenarios #13, #8, and #18 differ by their change in mean precipitation (0 %, -12.5 %, and +12.5 % of baseline values, respectively). Note that the color scale is identical for the three rightmost panels.

with warming across the scenarios. Furthermore, a more pronounced increase can be detected in the number of heat wave events over the southern portion of the basin. The average and maximum heat wave event duration presented in Fig. 6 shows how even 1 °C of warming can result in multi-day increases in both average and maximum heat wave duration at individual grid cells. The impacts are especially prominent on the maximum duration of heat waves, which can increase by more than 15 days per year for a scenario with 3 °C of warming.

Figs. 7-8 show how extreme precipitation and drought events vary across all the climate scenarios in Fig. 2 and Table 1, focusing only on one HUC-4 region (the San Joaquin basin, HUC4: 1804). In Fig. 7, we show how the 1-day and the 7-day largest precipitation events change with shifts in temperature and mean precipitation, all for an extreme precipitation scaling rate of 7% per °C. Similar to Fig. 4, we find that the 1-day precipitation maxima are largely insensitive to changes in mean precipitation, and instead only respond to changes in temperature that drive the absolute magnitude of extreme precipitation scaling. This is because the 1-day maxima are entirely determined by the upper tail of the daily distribution, which is controlled solely by the extreme precipitation scaling rate (see Fig. 3). While temperature changes and extreme precipitation scaling also dominate the rate of increase in 7-day maxima, changes in mean precipitation also have an effect, largely based on how they influence the smaller precipitation values during the 7-day

events. For the most intense scenario of change (5 $^{\circ}$ C of warming and a 25% increase in mean precipitation), the 7-day maxima increase by almost 38% over baseline values.

We focus on drought-of-record events of different durations in Fig. 8. Here, the results show that changes in mean precipitation dominate the change in drought magnitude for all durations, and the relationship is close to 1-to-1 (i.e., a similar percent change in mean precipitation is also seen for the change in drought magnitude). Interestingly, there is also a pronounced temperature effect on the magnitude for 1-year droughts, but this effect weakens for longer durations. This is caused by the same phenomenon described above, where for some change in mean precipitation, extreme precipitation scaling requires that lighter precipitation events be scaled downward (i.e., become even lighter) to compensate for increases in the extremes (also see Fig. 3). For 1-year droughts, this effect is more prominent, likely because 1-year droughts can occur with few or no heavy precipitation events, and so the downward scaling is experienced across most or all days in the 1-year drought. However, as drought durations grow longer, this temperature effect is dampened as more heavy and extreme precipitation events that have scaled upward are included in the long-duration drought periods.

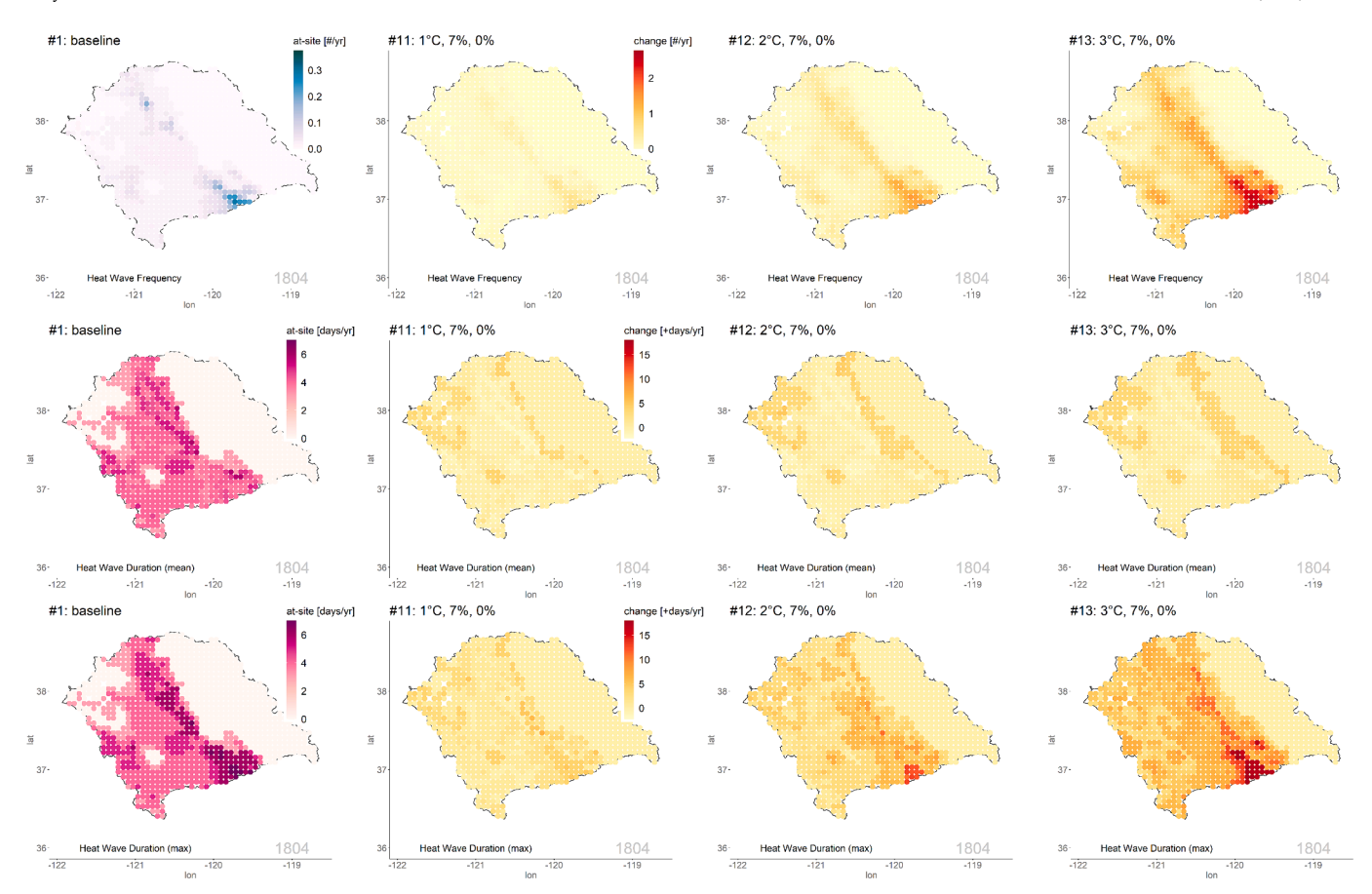


Fig. 6. (far-left column) At-site average frequency of heat wave events per year [number of events per year] (first row), as well as at-site mean (second row) and maximum (third row) of heat wave event duration per year [days of event per year] in the baseline scenario (no climate change). (middle-left to far-right columns) The change in the average frequency of heat wave events (number of additional events per year) and in the average and maximum heat wave event duration (longer event duration per year) are shown for three climate scenarios from Table 1, including scenarios #11, #12, and #13 with 1, 2, and 3 °C of warming, respectively, an extreme precipitation scaling rate of 7 % per °C, and 0 % change in mean precipitation. Note that the color scale is identical for the three rightmost panels in each row. All results are shown for the San Joaquin basin (HUC4: 1804).

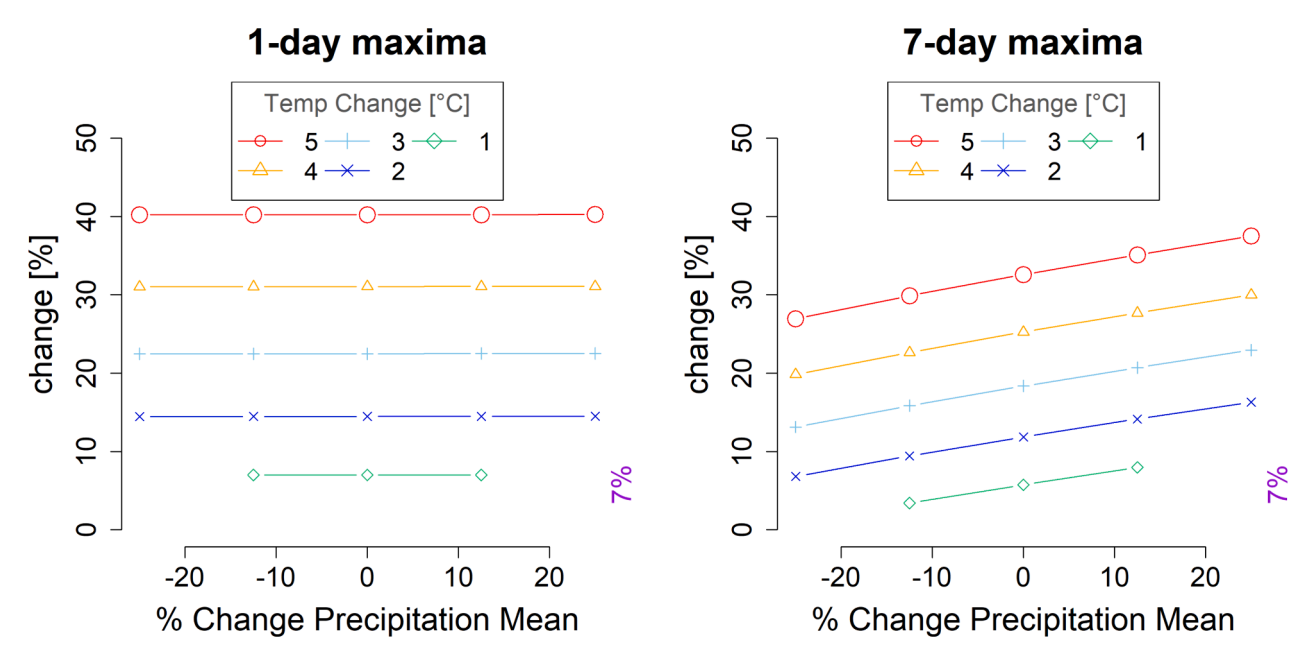


Fig. 7. Percent change from baseline for the largest (*left*) 1-day and (*right*) 7-day precipitation maximum. Changes are shown for five different scenarios of temperature change and five different scenarios of precipitation change, all with an extreme precipitation scaling rate of 7% per °C and for the San Joaquin basin (HUC4: 1804).

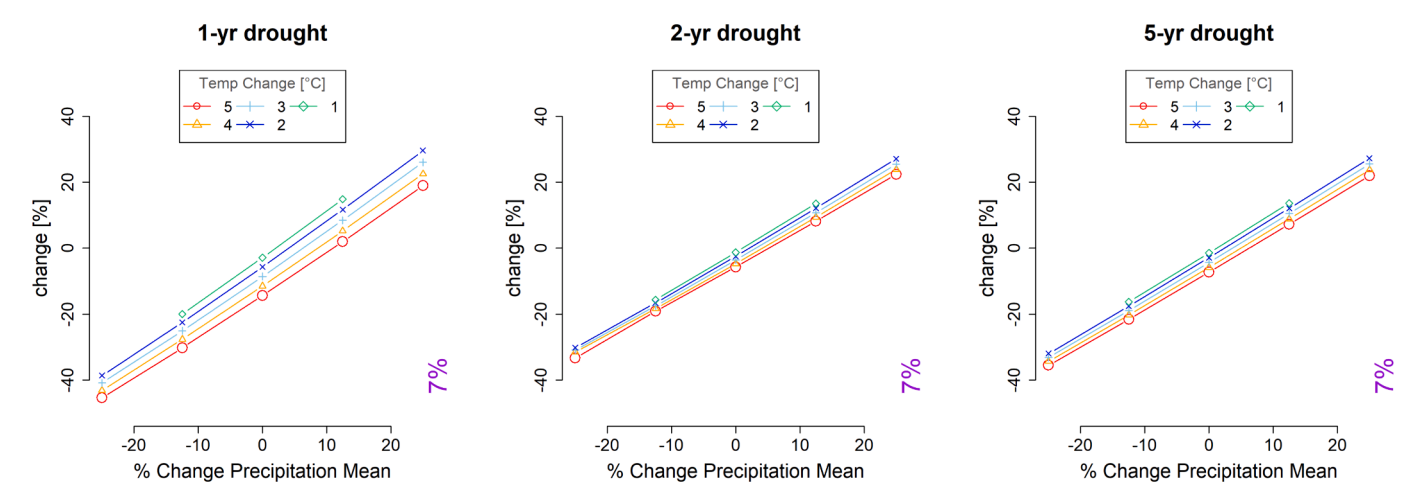


Fig. 8. Percent change from baseline for the worst (*left*) 1-year drought, (*middle*) 2-year drought, and (*right*) 5-year drought. Changes are shown for five different scenarios of temperature change and five different scenarios of precipitation change, all with an extreme precipitation scaling rate of 7% per °C and for the San Joaquin basin (HUC4: 1804).

3.2. Comparison against LOCA v.2 projections

In this section we provide a comparison between some of the thermodynamic climate scenarios generated by the weather generator and the ensemble of future projections in the recently released LOCA v.2 archive derived from CMIP6 (Pierce et al., 2023). We conduct this comparison in the Upper Tuolumne River basin, which is located within the San Joaquin HUC-4 region. LOCA v.2 is bias corrected and downscaled using the same historical observations as are used in the weather generator (Pierce et al., 2021), making a comparison between the two products more comparable.

To facilitate this comparison, we first took each climate model simulation from LOCA v.2 and identified the 30-year period in the future that exhibited an average of 2 $^{\circ}$ C of warming over the baseline period of 1981–2010 in the simulation. Using those 30 years for each simulation, we then concatenated these data across all model simulations, and compared them against the 1000-year stochastic weather generator simulation associated with climate scenario #12 in Table 1 (2 $^{\circ}$ C

warming, 0% change in mean precipitation, and 7% per °C scaling of extreme precipitation).

Fig. 9 focuses on the worst 1-, 2-, 3-, 4-, and 5-year drought events in the observed record, the LOCA v.2 data associated with 2 °C of warming, and the 1000-year weather generator simulation associated with climate scenario #12 from Table 1. More intense droughts than those historically observed can be seen in the 2 °C warming scenario for all durations in both the weather generator simulation and LOCA v.2. Drought intensification is linked to both natural variability under a longer record (1000 years for the weather generator; 3750 years for LOCA v.2), but also the suppression of low and moderate precipitation events under thermodynamic climate change during years that were already dry, as described earlier. For LOCA v.2, declines in the 2-year drought are more severe under 2 °C warming compared to the other durations, but this may be due to natural variability in the ensemble. Overall, the differences in drought intensity between the weather generator under a future 2 °C warming and LOCA v.2 projections around that same amount of warming are relatively small.

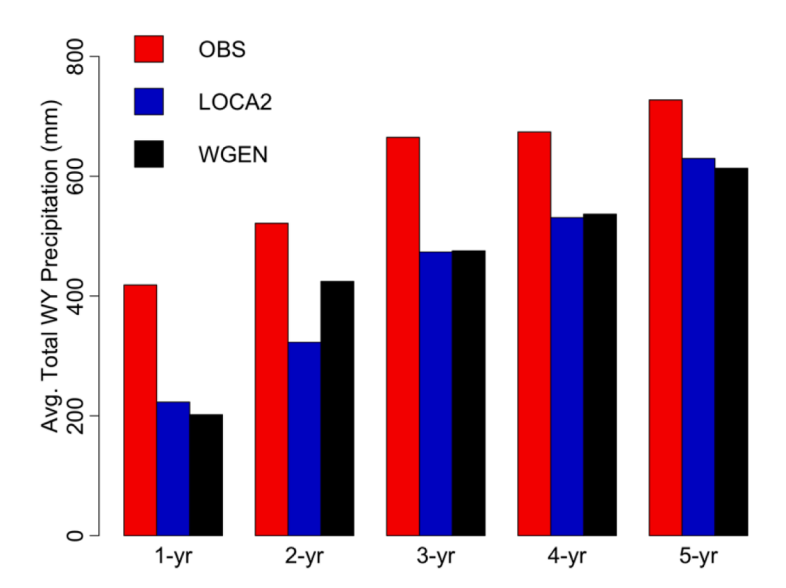


Fig. 9. The worst 1, 2, 3, 4, and 5-year drought events in the observed record (*red*), across the ensemble of future LOCA v.2 projections centered around 2 °C warming (*blue*), and in the 1000-year weather generator simulation for climate scenario #12 (2 °C warming, 0% change in mean precipitation, and 7% per °C scaling of extreme precipitation) (*black*). All results are shown for the Upper Tuolumne River basin. (For interpretation of the references to color in this figure legend, the reader is referred to the web version of this article.)

Another way to compare the weather generator simulations to LOCA v.2 is to quantify the relative contribution of the upper and lower quantiles of daily precipitation to long-term total precipitation. As shown in Dettinger (2016), historically, the wettest 5% of days contribute disproportionately to total annual precipitation, yielding a precipitation regime that is highly dependent on a few large storms at annual and interannual timescales. Thermodynamic precipitation scaling acts to amplify this regime, concentrating greater and greater portions of total precipitation into the largest storm events (and less and less into smaller to moderate-sized storms).

We explore this property for both the 1000-year weather generator simulation and the LOCA v.2 ensemble following methods applied in Dettinger (2016). First, all non-zero precipitation days (>0.01 mm) are extracted, averaged at the watershed basin scale, and split into the wettest 5% of precipitation days and all other precipitation days. This is done for the 50-year historical period 1950-1999 in each LOCA v.2 model-SSP-variant. For the weather generator, we break the 1000-year simulations into 20 non-overlapping 50-year blocks and split precipitation days in each block using the same approach. For the LOCA v.2 ensemble data, we extract 50-year periods from the projection period where the average temperature change (relative to 1981-2010) has reached incremental warming levels of 1 °C, 2 °C, 3 °C, and 4 °C, and split those daily precipitation accordingly. Finally, for each 50-year precipitation block of the weather generator and LOCA v.2 ensemble, the change in precipitation of the wettest 5% of days and all other days is divided by the total historical precipitation, thus yielding the contribution of each quantile to the total precipitation change in a 50-year block.

Fig. 10a shows the results of this analysis for weather generator scenario #12 compared to the current condition scenario #1 (i.e., no perturbation). The effect of thermodynamic scaling is visible and mostly equivalent for all 50-year blocks: the contribution of the wettest 5% of days to total precipitation is $\approx\!5\%$ higher (and all other days $\approx\!5\%$ lower) under 2 °C warming. For example, in the 50-year block which has $\approx\!13\%$ more total precipitation compared to historical, the wettest 5% of days contribute 9% (14%) without (with) thermodynamic scaling, while all other days contribute 4% (-1%) without (with) thermodynamic scaling. In other words, the scaling of extreme precipitation has made it so that overall wetter periods have become wetter due only to large storm events, while overall drier periods have become drier due mostly to "losing" precipitation from small to moderate sized storms.

Fig. 10b shows the results of this analysis for weather generator scenario #12 compared to that of the LOCA v.2 ensemble at the average warming of 2 °C. The LOCA v.2 ensemble does not show the same level of extreme precipitation scaling as used in the weather generator, thus changes in contributions from the wettest 5% and all other days in overall wetter and drier 50-year periods are not as severe as those generated in scenario #12. Similarly, Fig. 10c compares the weather generator and LOCA v.2 for each incremental warming level between 1–4 °C, showing that the rate of extreme precipitation scaling is not as high in LOCA v.2 as is assumed in the weather generator scenarios, which reaches approximately twice that of LOCA v.2 at the 4 °C warming level.

These results suggest two important takeaways: 1) thermodynamic scaling as applied in the weather generator produces an effect on overall wetter and drier precipitation regimes where more (less) of total precipitation is derived from large (small to moderate) storms; 2) the rate of thermodynamic scaling (7% per °C) might be considered a conservative assumption relative to what is shown in the LOCA v.2 ensemble. The latter may be attributable to both biases in the LOCA v.2 statistical downscaling product and the presence of reduced rates of extreme precipitation scaling due to underlying and counteracting effects of atmospheric thermodynamics and dynamics (Gu et al., 2023).

3.3. Exploration of dynamic climate changes

The results in Sections 3.1 and 3.2 are based on climate scenarios that were largely developed from a thermodynamic perspective, i.e., changes in extreme precipitation that are tied to changes in the moisture holding capacity of the atmosphere under warming. The changes in mean precipitation could be considered partially thermodynamically driven, although not entirely. In this section, we consider climate changes that are entirely dynamic in nature, in that they are driven only by changes in atmospheric circulation.

As discussed in Section 2.2, we select two dynamic climate scenarios based on recent trends in WR frequencies over the 72-year historical record. Fig. 11 shows these trends for the 10 WRs considered in this work. A red asterisk is used to highlight those WRs with significant trends at the 1% significance level. WRs 3, 8, 9, and 10 all exhibit significant trends at this level. Recall that WRs 1–7 are cold season WRs, while WRs 8–10 occur in the warm season. As the vast majority of precipitation occurs in the cold season, the increased frequency of WR3

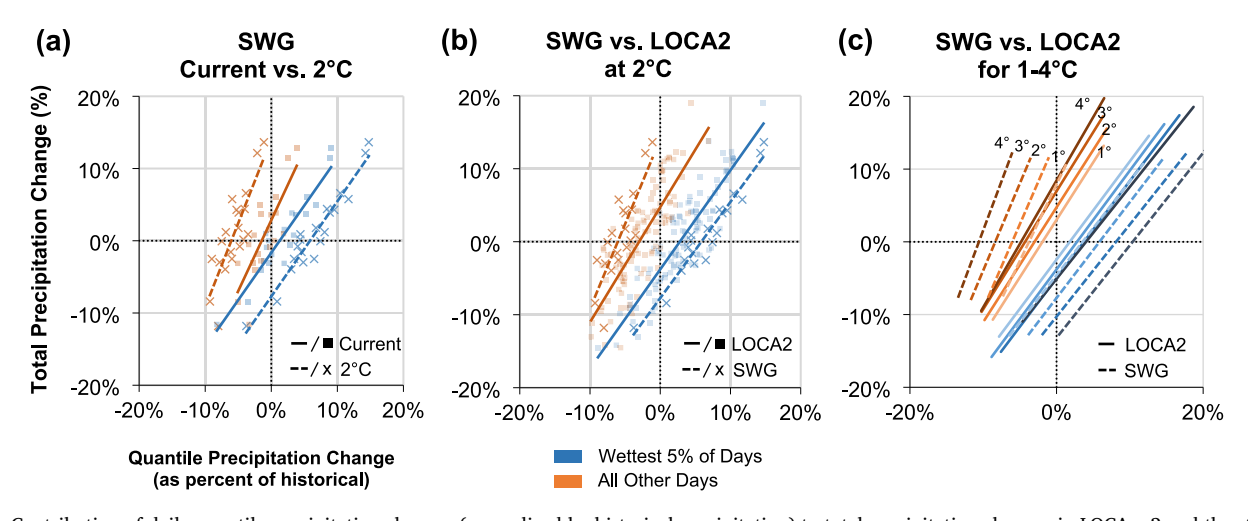


Fig. 10. Contribution of daily quantile precipitation changes (normalized by historical precipitation) to total precipitation changes in LOCA v.2 and the stochastic weather generator (SWG), where **(a)** compares the 20, 50-year blocks of the 1000-year weather generator simulation under current climate (scenario #1) to the simulation from scenario #12 (2 °C warming, 0 % change in mean precipitation, and 7 % per °C scaling of extreme precipitation); **(b)** compares the scenario #12 weather generator simulation to the ensemble of LOCA v.2 projections centered around 2 °C warming; and **(c)** compares the trends of weather generator simulations (scenario #11, #12, #13, and #14) and the ensemble of LOCA v.2 projections centered around 1 °C, 2 °C, 3 °C, and 4 °C warming. All results are shown for the Upper Tuolumne River basin.

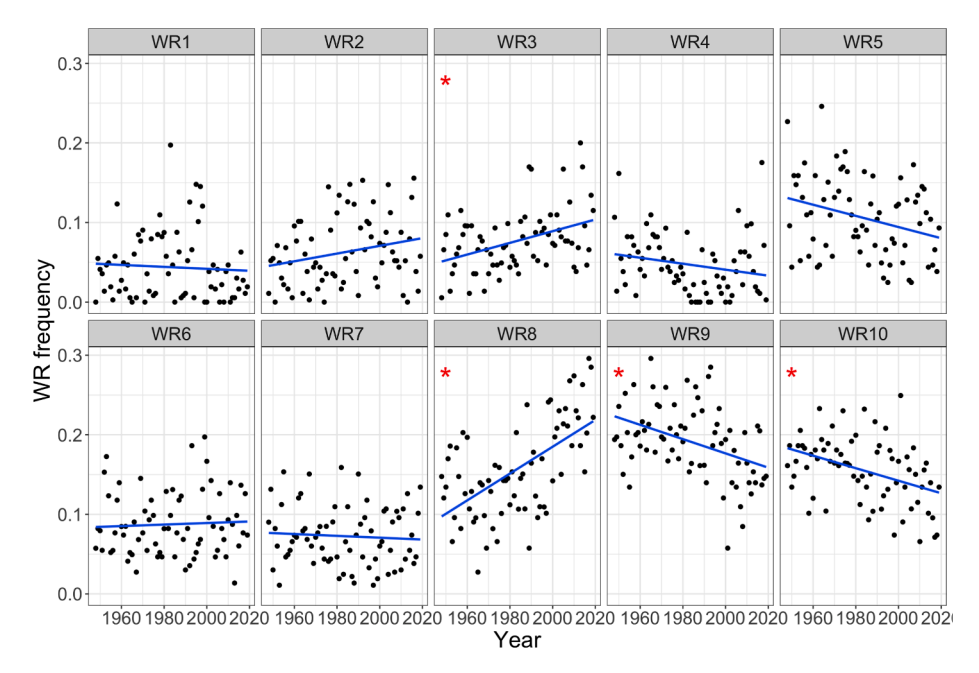


Fig. 11. Historical trends in each of the 10 WRs. The blue line indicates a linear regression of WR frequency against time. Significant trends at the 1% significance level are denoted by a red asterisk (*). (For interpretation of the references to color in this figure legend, the reader is referred to the web version of this article.)

has the largest implications for recent changes in California weather. WR3 is characterized by a ridge over western North America and is associated with dry conditions across California. The recent increases in WR3 are consistent with the 2-decade long drought conditions experienced over California since 2000. While we do not attempt explain the causes of the WR trends observed here, we do note that recent attribution studies have highlighted possible explanations for such trends, including anthropogenic warming (Zhang et al., 2022) and rising aerosol emissions across southeast Asia (Kuo et al., 2023).

Based on the trends in Fig. 11, we consider two dynamic climate change scenarios to explore. In the first scenario (Dynamic Scenario #1), we simulate from the stochastic weather generator after adjusting the long-term mean frequency of WR3 upwards from its 1948-2019 mean (\sim 7.7% of days) to its end of record average (\sim 10% of days), and adjust the frequency of all other WRs uniformly downward to accommodate this change. This represents an approximate 30% increase in the frequency of days classified as WR3 (see Appendix A.2 for methods on how this change is implemented in the simulation process). Given the association between WR3 and dry conditions in California, we anticipate this climate change scenario will lead to worsening droughts and possibly a reduction in extreme precipitation events, although the magnitude of the effect is unclear a priori. We will juxtapose the effects of this climate change scenario to one scenario from those listed in Table 1 (scenario #8 with 3 °C of warming, extreme precipitation scaling of 7% per °C, a -12.5% change in mean precipitation) as a point of comparison. We will also combine these two scenarios to see their joint impact, i.e., a scenario with 30% more frequent WR3 days along with 3 °C of warming, extreme precipitation scaling of 7% per $^{\circ}\text{C}\text{,}$ and a -12.5% change in mean precipitation.

In the second dynamic climate change scenario (Dynamic Scenario #2), we shift the frequency of all WRs (not just WR3) to their average frequency at the end of the period of record, based on regression estimates for the last year on record from a linear regression against time (i. e., the value estimated by the blue line in Fig. 11 for the year 2019). Therefore, recent trends in any WR (significant or not) will be reflected in the weather simulated by the stochastic weather generator. This dynamic climate change scenario implicitly assumes that the atmospheric circulation experienced more recently reflects a "new normal" that will persist over the next several decades. Importantly, we emphasize here

that these dynamic climate change scenarios should not be interpreted as confident projections of what will happen to atmospheric circulation under climate change, but rather as "what if" scenarios that allow us to explore the potential impact of these types of change to decision-relevant climate statistics over areas in California. The results of this exploration will help determine how important such dynamic climate changes could be to water systems planning and management throughout the state, which would provide insight into the degree of effort that should be expended in resolving uncertainties around these types of future climate change.

Fig. 12 shows the impact of Dynamic Scenario #1 (a 30% increase in the frequency of WR3) on drought, specifically the magnitude of the worst 5th percentile 2-year, 3-year, and 5-year droughts on record (i.e., the 5th percentile of all 2-year, 3-year, and 5-year water-year precipitation totals across the 1000-year record). Four scenarios are shown, including a baseline (no climate change), Dynamic Scenario #1 (termed 'dynamic change'), the results from Scenario #8 in Table 1 (termed 'thermodynamic change'), and the combined scenario where the changes in Scenario #8 in Table 1 are imposed on the weather generator output forced with a 30% increase in WR3 frequency (termed 'both'). The results show that for shorter duration droughts (2-year, 3-year), the dynamic climate change scenario has more intense droughts compared to the baseline, but the impact is not as intense as that of the thermodynamic scenario. However, for long-duration droughts (5-year), the impact of the dynamic climate change scenario is very similar compared to that of the thermodynamic scenario. This suggests that for intense long-duration droughts, the importance of a single WR (and the synoptic scale atmospheric flow pattern it represents) becomes increasingly important, likely because the increased frequency of that pattern has more time to manifest in the long-term droughts. When both scenarios are combined, droughts become even more intense; for the 3-year drought, the precipitation total of the drought under the baseline declines by 22% under the combined scenario.

Fig. 13 shows similar results to Fig. 12, but for the 20-year and 100-year extreme 1-day precipitation event estimated from a GEV distribution fit to annual maxima. Here, we see that an increase in frequency in WR3 has a small negative effect on both the 20-year and 100-year storm, as compared to the baseline. However, the magnitude of this effect is small, especially when compared to the increase in these design events

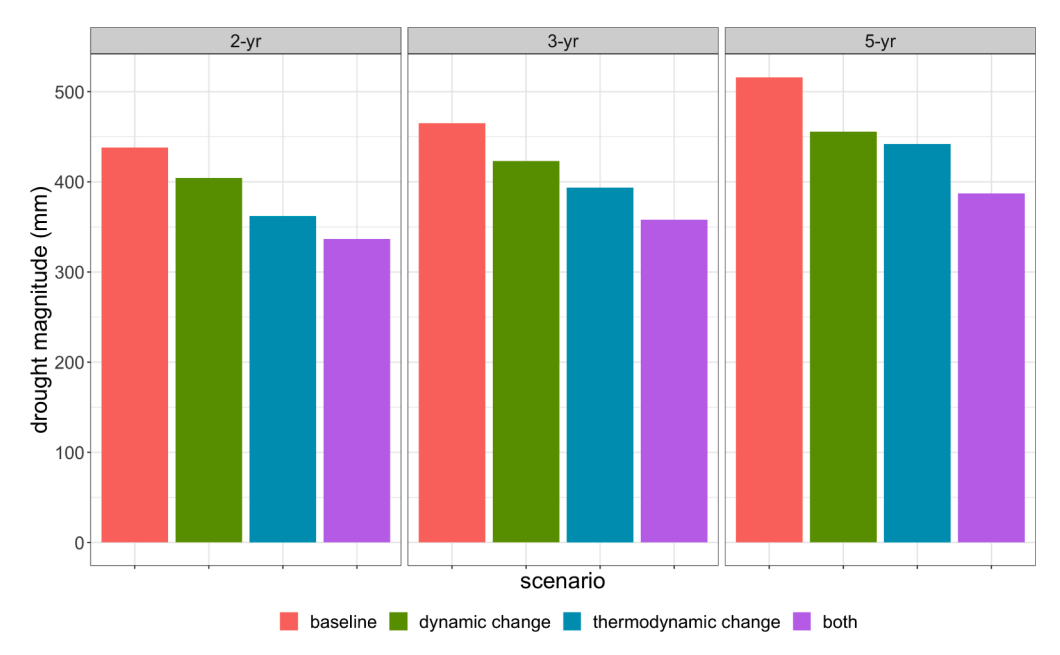


Fig. 12. The total precipitation during the worst 5th percentile 2-year, 3-year, and 5-year drought from the baseline scenario (no climate change), Dynamic Scenario #1 ('dynamic change'), Scenario #8 in Table 1 ('thermodynamic change'), and the combined scenario where the changes in Scenario #8 in Table 1 are imposed on Dynamic Scenario #1 ('both'), for the San Joaquin basin (HUC4: 1804).

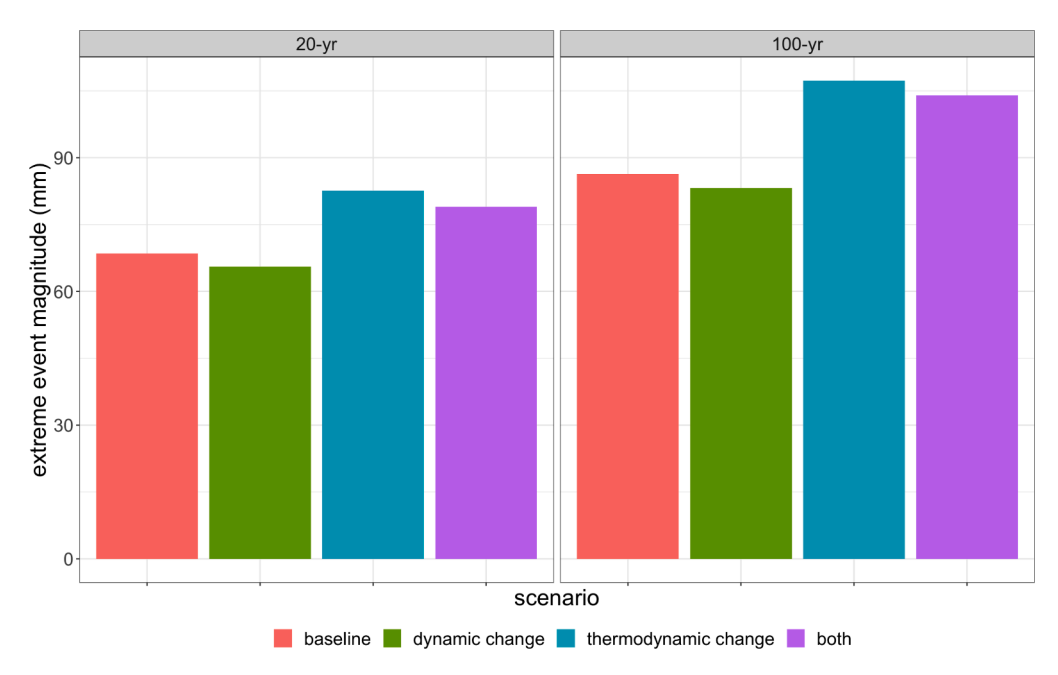


Fig. 13. The magnitude of the 20-year and 100-year 1-day extreme precipitation event from the baseline scenario (no climate change), Dynamic Scenario #1 ('dynamic change'), Scenario #8 in Table 1 ('thermodynamic change'), and the combined scenario where the changes in Scenario #8 in Table 1 are imposed on Dynamic Scenario #1 ('both'), for the San Joaquin basin (HUC4: 1804).

under the thermodynamic scenario with extreme precipitation scaling with warming. The combined effect of these two scenarios appears additive, with design events that are slightly smaller than the thermodynamic scenario but still much larger than the baseline.

Figs. 14-15 show the same results as Figs. 12-13, but for Dynamic Scenario #2 (i.e., the most recent frequencies for all WRs based on regression estimates against time). Similar to Dynamic Scenario #1, the results in Fig. 14 show that droughts generally become more intense under Dynamic Scenario #2. However, the effect is not as apparent as compared to that seen in Fig. 12, especially for the shorter duration droughts (2-year, 3-year). Conversely, the results in Fig. 15 show that

the propagation of trends in all WRs has a large negative effect on both the 20-year and 100-year storm, as compared to the baseline. This effect is much stronger than that seen for Dynamic Scenario #1 (Fig. 13). Therefore, the results for Dynamic Scenario #2 suggest that by propagating recent trends in all WRs into the weather generator, the resulting simulations are slightly drier than the baseline on average, but reductions in extreme events are significant. The reasons for these differences with Dynamic Scenario #1 are not immediately clear, but they do suggest that shifting frequencies in multiple WRs at once can result in complex dynamics and emergent climate changes in decision-relevant metrics that are difficult to anticipate *a priori*.

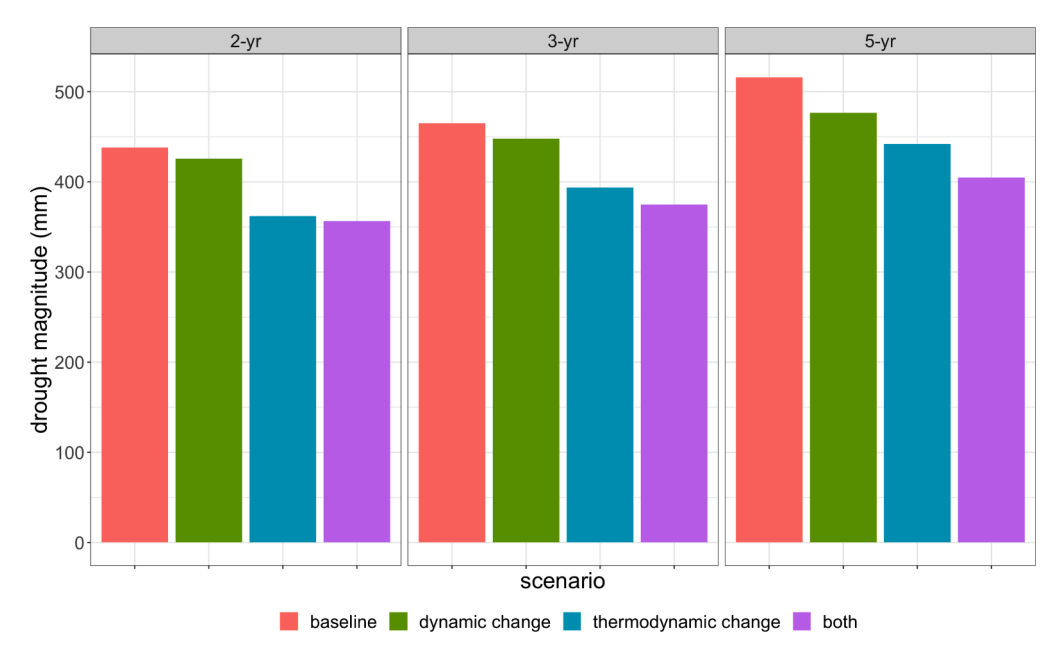


Fig. 14. The total precipitation during the worst 5th percentile 2-year, 3-year, and 5-year drought from the baseline scenario (no climate change), Dynamic Scenario #2 ('dynamic change'), Scenario #8 in Table 1 ('thermodynamic change'), and the combined scenario where the changes in Scenario #8 in Table 1 are imposed on Dynamic Scenario #2 ('both'), for the San Joaquin basin (HUC4: 1804).

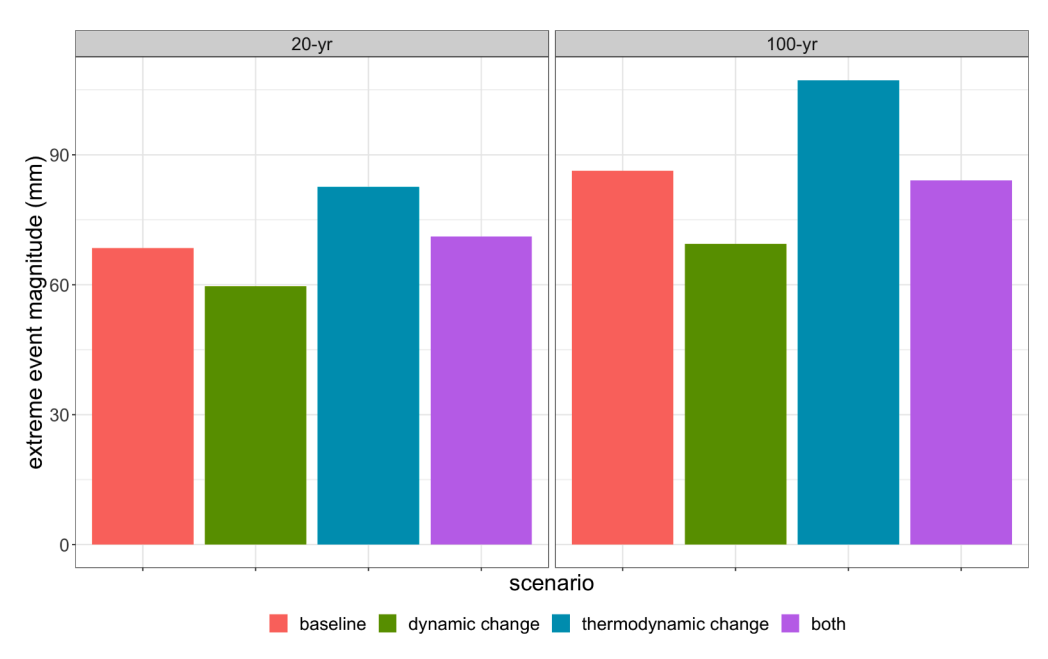


Fig. 15. The magnitude of the 20-year and 100-year 1-day extreme precipitation event from the baseline scenario (no climate change), Dynamic Scenario #2 ('dynamic change'), Scenario #8 in Table 1 ('thermodynamic change'), and the combined scenario where the changes in Scenario #8 in Table 1 are imposed on Dynamic Scenario #2 ('both'), for the San Joaquin basin (HUC4: 1804).

4. Conclusions, final remarks, and guidance for use

This work presented the second of a two-part series of studies demonstrating the application of a stochastic weather generator for the development of gridded climate change scenarios across the entire state of California. The model was used to create a 30-member ensemble of 1000-year climate scenarios that primarily reflect thermodynamic climate changes, including temperature increases and the scaling of extreme precipitation with temperature, as well as additional changes in mean precipitation. A limited set of proof-of-concept dynamic climate change scenarios were also developed with the stochastic weather generator that represent shifts in the frequency of major atmosphere

circulation patterns. By developing thermodynamic and dynamic climate change scenarios separately, water managers are able to use the generated data from this work to systematically explore the sensitivity of their systems to various types of climate change. The results of such vulnerability analyses would then empower water managers to work more closely with the climate science community to understand the likelihood of climate futures that threaten the reliability of water services, thereby providing more direct information to support adaptation decision-making.

One benefit of the weather generator is that it can efficiently generate long records of weather data (1000's of years) that are useful for uncovering climate vulnerabilities in water systems. However, there

are currently limitations in the way the model can be used to generate scenarios of future climate. For example, when imposing thermodynamic climate changes in which the distribution of daily precipitation is stretched, the weather generator scales up extreme precipitation events and scales down light to moderate events. However, it does not change the frequency of precipitation occurrence (i.e., more zero precipitation days). Future adjustments to the model are needed to be able to impose this change directly in scenario development. One possibility for this would be the introduction of an autologistic regression model that can simulate the occurrence of spatially correlated zero and non-zero precipitation. The parameters of this model could then be perturbed directly to create scenarios of more frequent zero precipitation days.

A broader limitation of the weather generator is that all scenarios generated with the model must be explicitly specified by the analyst. That is, the weather generator will – by design – only create scenarios of future climate that it is directed to create. This is in direct contrast to GCMs, where the governing physics of the Earth system and specified boundary conditions (i.e., emission scenarios) lead to plausible scenarios that emerge through internal, interacting processes within the model. This difference is critical in highlighting how the weather generator should (and should not) be used to support climate change adaptation planning.

In the context of climate change adaptation planning for water systems, scenarios of future climate created by the weather generator should be viewed as complementary to, rather than in competition with, other downscaled climate projections from GCMs. The weather generator cannot replace GCMs, which are the primary tool for uncovering robust signals of climate change. Rather, the weather generator is designed to provide flexibility in scenario development, so that water resource planners and engineers can first openly communicate with the climate science community about which signals within GCM projections are most robust or worthy of focused attention. After those signals have been identified, they can be embedded into climate traces from the weather generator in a way that is tailored to support planning efforts. For example, water resources planning often requires many models in sequence (e.g., hydrologic, reservoir operations, hydraulic, and groundwater models), many of which can be computationally demanding. The high computational expense often precludes using all data from an entire ensemble of downscaled GCM projections. However, with the weather generator an analyst can quickly create 1000's of years of weather meant to represent a pre-specified set of climate change signals, and then can select a subset of that trace of an arbitrary length (e.g., 100 years) that i) is limited in length and so computationally feasible for complex modelling chains; and ii) contains both robust climate change signals and also plausible but challenging extreme events useful for stress testing water system performance. This functionality can support robust climate change adaptation planning in a way that leverages state-of-the-science climate understanding while also accommodating the constraints of typical water resources planning studies.

We envision the process above to be iterative, in which new knowledge derived from climate change projections or emerging observations can quickly be incorporated into new scenarios with the weather generator. For example, in Fig. 10, results from the LOCA v.2 ensemble suggest that a smaller scaling rate of extreme precipitation with warming (i.e., less than 7% per °C) may be warranted. This is also supported by a similar result based on a very recent observational study of extremes in California (Najibi and Steinschneider, 2023). The climate scenarios developed in this work mostly assume a more conservative 7% per °C in extreme precipitation scaling. However, it is straightforward to generate new sets of climate scenarios with a lower scaling rate, based on the knowledge revealed through the analysis of LOCA v.2 and observational records. These new scenarios can be generated quickly (in a matter of hours to days, depending on the spatial scale of the analysis). In this way, the weather generator can be used as a tool to shorten the period between climate knowledge generation and data production to

support planning. One could take a similar approach using other downscaled climate projection products besides LOCA v.2 (e.g., MACA, STAR-ESDM; Abatzoglou and Brown, 2012; Hayhoe et al., 2023), which would enable the creation of climate scenario ensembles with a single approach (the weather generator) that contain differences in key climate change signals from various downscaling methods. If paired with rainfall-runoff and water systems models, this approach would help assess whether such differences in climate signal matter from the perspective of water resources impacts.

For the data developed and presented in this work, stakeholders can utilize the 1000-year weather generator trace under 30 different climate scenarios to infer the joint impact of both climate change and natural climate variability on their systems. We recommend that stakeholders use these different data products in stages to help develop robust adaptations of water resources infrastructure under climate change. For example, initial adaptation strategies (e.g., new reservoir operational policies; new infrastructure of managed aquifer recharge) could be developed using the baseline record to ensure these strategies are able to meet performance requirements under past and recent extreme events. Then, these strategies could be re-evaluated using the 30 climate change scenarios for the 1000-year weather generator simulation. These evaluations would provide information on how robust a given adaptation strategy is to climate change, natural climate variability, and a combination of the two.

Such information could be used in different ways to alter the initial adaptation strategy. For instance, if a strategy appears vulnerable to the 1000-year baseline weather generator simulation (i.e., natural climate variability) or likely future climate scenarios (e.g., a low degree of future warming projected in most GCMs over the next few decades), this might suggest an immediate need for a more robust strategy. Alternatively, in cases where an adaptation strategy is only vulnerable to the most extreme climate change scenarios or to certain climate change scenarios coupled with the longer (and more extreme) weather generator simulation, the current adaptation strategy may be deemed adequate if coupled with plans for continued climate monitoring and retrofits/adjustments that could be implemented later if needed.

CRediT authorship contribution statement

Nasser Najibi: Conceptualization, Data curation, Formal analysis, Investigation, Methodology, Validation, Visualization, Writing – original draft, Writing – review & editing. Alejandro J. Perez: Data curation, Resources, Validation. Wyatt Arnold: Data curation, Resources, Validation. Andrew Schwarz: Resources, Software, Validation. Romain Maendly: Project administration, Resources, Software, Validation. Scott Steinschneider: Conceptualization, Formal analysis, Funding acquisition, Investigation, Methodology, Project administration, Supervision, Validation, Writing – original draft, Writing – review & editing.

Declaration of competing interest

The authors declare that they have no known competing financial interests or personal relationships that could have appeared to influence the work reported in this paper.

Data availability

The climate change scenarios developed under this work are publicly available and can be retrieved from the California Department of Water Resources, who sponsored this work (https://data.cnra.ca.gov/dataset, look up 'weather generator', i.e., https://data.cnra.ca.gov/dataset/ca-weather-generator-gridded-climate-pr-tmin-tmax-2023).

Acknowledgements

This work was supported by the California Department of Water Resources and Turlock Irrigation District. This project was also partially supported through funds provided under NSF Award No. 2205239. We would like to acknowledge valuable feedback on this work from Alexander Weyant and Alexander Gershunov at the Scripps Institution of Oceanography, UC San Diego.

Appendix A. Mathematical formulation of the stochastic weather generator

A.1. Thermodynamic climate changes to extreme precipitation using the Gamma-GPD extreme mixture model

We use quantile mapping to shift and stretch the distribution of daily, non-zero precipitation in a way that replicates the effects of warming temperatures on precipitation through increases in the moisture holding capacity of the atmosphere. In this approach, we must first specify a target value for daily average precipitation and a target scaling for extreme precipitation events under a particular future scenario. For instance, let $\mu^* = (1+\omega)\mu$ be the desired mean for a future climate scenario such that μ^* is $\omega \times 100\%$ greater than the historic mean μ , and let $(1+\eta)^{\Delta T}$ be the target scaling rate for extreme precipitation events, where $\eta \times 100\%$ is the percentage increase in extremes per °C of warming. In this work we assume the same mean change for every calendar month, although a different change for each month is also permissible.

In the weather generator, we resample daily precipitation via a block bootstrap to develop an initial simulation and then adjust heavy precipitation values with a copula-based jittering algorithm and a gamma-GPD extreme mixture model to develop previously unexperienced extreme events. Here, we expand that jittering algorithm and adjust the parameters of the gamma-GPD extreme mixture model to impose the changes to mean and extreme precipitation specified above.

This procedure follows two main steps. First, for all precipitation values that are designed as heavy events (i.e., precipitation $p_{s,t}$ at site s and time t is greater than the site-specific threshold ζ_s), we assume that these values will scale at the rate $(1+\eta)^{\Delta T}$. Therefore, these heavy precipitation values will first be jittered and then multiplied by $(1+\eta)^{\Delta T}$.

Second, all other non-heavy precipitation values must be adjusted so that 1) the entire series of both non-heavy and heavy precipitation have a new mean μ^* ; and 2) non-heavy precipitation values that approach the threshold ζ_s are also scaled upward so that they approach an asymptotic scaling of $(1+\eta)^{\Delta T}$. To do this, we infer new parameters for the gamma component of the gamma-GPD extreme mixture model and then impose quantile mapping on resampled, non-heavy precipitation through that gamma component.

Let $\alpha_{s,m}$, $\beta_{s,m}$ be the parameters of a gamma distribution fit to non-zero, non-heavy precipitation at site s in calendar month m, let σ_s , ξ_s be the parameters of a GPD distribution fit to heavy precipitation values at site s greater than the threshold ζ_s , and let $\pi_{s,m}$ be the probability of precipitation exceeding the threshold ζ_s (which can vary by month). The mean of the GPD distribution is given by $\mu_{GPD} = \zeta_s + \frac{\sigma_s}{1-\xi_s}$, which becomes

$$\mu_{\textit{GPD}^{\circ}} = (1+\eta)^{\Delta T} \Big(\zeta_{\textit{s}} + \frac{\sigma_{\textit{s}}}{1-\xi_{\textit{s}}}\Big)$$
 after the extreme event scaling is applied in step 1 to all heavy precipitation events. Therefore, if the ultimate goal is to

develop daily non-zero precipitation with a new mean of μ^* , then the mean of a new gamma distribution μ_{gamma^*} needs to take into consideration the new mean of the heavy precipitation under the scaled GPD. Thus, we derive a scaling factor $(1+\delta)$ for the mean of the gamma distribution (μ_{gamma}) fit to the original non-heavy precipitation data as follows:

$$(1+\delta) = \frac{(1+\omega)(1-\pi_{s,m})\mu_{gamma} - \left[(1+\eta)^{\Delta T} - (1+\omega)\right]\pi_{s,m}\mu_{GPD^*}}{(1-\pi_{s,m})\mu_{gamma}}$$
(A1.1)

$$\mu_{\text{gamma}^*} = (1+\delta)\mu_{\text{gamma}} \tag{A1.2}$$

Here, $\delta \times 100\%$ represents a required percentage change in the gamma distribution's mean so that, after accounting for the new mean of the heavy precipitation under the scaled GPD (μ_{GPD}), the new mean of all non-zero precipitation (μ^*) will be $\omega \times 100\%$ of the original mean μ .

We then identify new parameters α^*, β^* for the gamma distribution by optimizing a multiplicative factor ρ as follows:

$$\min_{\rho} \left(\frac{F_{gamma}^{-1}(q|\alpha^*, \beta^*)}{F_{gamma}^{-1}(q|\alpha, \beta)} - (1+\eta)^{\Delta T} \right)^2 \tag{A1.3}$$

such that

$$\alpha^* = \alpha(1+\delta)\rho$$

$$\beta^* = \beta \rho$$

Here, $\mu_{gamma^*} = \frac{a^*}{\beta^*} = \frac{a(1+\delta)\rho}{\beta\rho} = (1+\delta)\mu_{gamma}$, guarantying the correct change to the mean of the gamma distribution. The optimization then selects ρ and subsequently α^*, β^* in order to minimize the squared difference between the target change in extreme precipitation $\left((1+\eta)^{\Delta T}\right)$ and the ratio of quantile functions of the new and old gamma distributions for some quantile q. We set q equal to some very large quantile (e.g., 0.9999999) so that the optimization tries to find new gamma parameters α^*, β^* that force the tail of the gamma distribution (i.e., the very largest non-heavy precipitation events) to scale at the same rate as the heavy precipitation events.

Once the new gamma parameters are determined for each site and month, daily simulated non-heavy precipitation $\widetilde{p}_{s,t}$ from the bootstrap is adjusted by first determining the non-exceedance probability $\widetilde{u}_{s,t_{gamma}} = F_{gamma}\left(\widetilde{p}_{s,t} \mid \alpha, \beta\right)$, and then replacing the resampled precipitation value with a new value derived from the adjusted gamma distribution:

 $F_{gamma}^{-1}\left(\widetilde{u}_{s,t_{gamma}} \mid \alpha^*, \beta^*\right)$. This procedure is repeated for each nonzero, non-heavy precipitation amount for each site synthesized by the weather generator.

A.2. Non-parametric simulation of weather regimes for dynamic climate change

Following the approach present in Part (1) related to non-parametric simulation of WRs for baseline weather, the probabilities p_n can be then adjusted to alter the frequencies of each of the K WRs in the final sequence of WR simulation, enabling the generation of dynamic climate change scenarios (i.e., scenarios in which the frequencies of different atmospheric flow patterns change compared to their historical frequencies). This is achieved using a linear program. The goal of this model is to identify new sampling probabilities p_n that, when used in the nonparametric simulation approach above, create a sequence of WRs with long-term average frequencies that approach some vector of target frequencies $\theta^* = \{\theta_1^*, \dots, \theta_K^*\}$ which define a scenario of dynamic climate change.

Let $\theta_{i,n}$ be the average frequency of occurrence (expressed as a probability) of WR i occurring in segment n. This value can be calculated simply by adding up the historical number of daily WR i occurrences in segment n and dividing it by the total number of days in the segment. We develop a series of K equations (for the K WRs) relating the WR frequencies in each segment to the target frequencies θ^* based on the sampling probabilities of each segment, as follows:

$$p_{1}\theta_{1,1} + \dots + p_{n}\theta_{1,n} + \dots + p_{N_{D}}\theta_{1,N_{D}} - \pi_{1}^{+} + \pi_{1}^{-} = \theta_{1}^{*}$$

$$\vdots$$

$$p_{1}\theta_{K,1} + \dots + p_{n}\theta_{K,n} + \dots + p_{N_{D}}\theta_{K,N_{D}} - \pi_{K}^{+} + \pi_{K}^{-} = \theta_{K}^{*}$$
(A2.1)

Here, π_i^+ and π_i^- are slack variables for the i^{th} WR, which allow the weighted average frequency across the N_D segments to deviate from the target frequency θ_i^* . We also require that the sampling probabilities across segments sum to unity:

$$p_1 + \dots + p_n + \dots + p_{N_D} = 1 \tag{A2.2}$$

We seek to minimize the slack variables π_i^+, π_i^- for i=1,...,K in the objective function in order to force the solution to find sampling probabilities $\{p_1, \cdots, p_{N_D}\}$ that help achieve the target WR frequencies θ^* :

$$J_1 = \sum_{i=1}^{K} C_{\pi} \left(\pi_i^+ + \pi_i^- \right)$$
 (A2.3)

where J_1 is the first component of the objective function to be minimized, and C_π is a cost coefficient. If the model is defined only by the constraints in Eqs. (A2.1)-(A2.2) and the objective function in Eq. (A2.3), there can be a tendency for the solution to force the sampling probabilities for many segments towards zero, and applying non-zero probability to only a handful of segments. This is undesirable, because we do not want to repeat only a few D-year segments of daily WRs in our final simulation. Therefore, we further adjust the model to incentivize equal sampling probabilities across segments (i.e., minimize the deviation of p_n from $\frac{1}{N_D}$) as much as is possible while still achieving long-term WR frequencies that approach the target values θ^* . To do this, we introduce a series of additional constraints on the sampling probabilities themselves:

$$p_n - \gamma_n^+ + \gamma_n^- = \frac{1}{N_D} \tag{A2.4}$$

Here, γ_i^+ and γ_i^- are slack variables for the n^{th} sampling probability that quantify its deviation from a uniform probability $\frac{1}{N_D}$. Each slack variable is further partitioned into two components that can be minimized in the objective function, allowing for a piecewise linear cost function on these deviations:

$$\gamma_n^+ = \gamma_{n,1}^+ + \gamma_{n,2}^+ \gamma_n^- = \gamma_{n,1}^- + \gamma_{n,2}^- \tag{A2.5}$$

And:

 $\gamma_{n,1}^+ \leq \tau_{\gamma}$ for all $n \in \{1, \dots, N_D\}$

$$\gamma_{n,1}^- \le \tau_\gamma$$
 (A2.6)

With

$$J_2 = \sum\nolimits_{n = 1}^{{N_D }} {\left({{C_{{\gamma _1}}}\gamma _{n,1}^ + + {C_{{\gamma _1}}}\gamma _{n,1}^ - + {C_{{\gamma _2}}}\gamma _{n,2}^ + + {C_{{\gamma _2}}}\gamma _{n,2}^ - } \right)} \tag{A2.7}$$

Here, J_2 is the second component of the objective function to be minimized, such that the final objective function is $J = J_1 + J_2$. τ_{γ} is a user-selected threshold, and C_{γ_1} and C_{γ_2} are cost coefficients such that $C_{\gamma_2} \gg C_{\gamma_1} \gg C_{\pi}$. This formulation will seek solutions that drive the sampling probabilities p_n towards a uniform probability $\frac{1}{N_D}$, and will penalize small deviations from $\frac{1}{N_D}$ (i.e., deviations smaller than τ_{γ}) less than large deviations. Both C_{γ_2} and C_{γ_1} are significantly greater than C_{π} , which will force the model to prioritize keeping the sampling probabilities close to $\frac{1}{N_D}$ over adjusting the sampling probabilities to achieve the target WR frequencies θ^* . To force the model to achieve WR frequencies that are close to the target, we also constrain the slack variables π_i^+ and π_i^+ with a user-defined threshold (τ_{π}) to ensure that the weighted average frequency across the N_D segments is within some small distance of the target for all WRs, as below:

for all
$$i \in \{1, \dots, K\}$$
,
$$\begin{aligned}
\pi_i^+ &\leq \tau_\pi \\
\pi_i^- &\leq \tau_\pi
\end{aligned}$$
(A2.8)

The value of τ_{π} can be set small at first (e.g., 0.0001) and iteratively adjusted upward if the model is initially infeasible. τ_{π} can be further adjusted upward to strike a balance between achieving the target WR frequencies and retaining sampling probabilities for each segment that are close to a

uniform probability. This balance is ultimately subjective and left to the analyst to decide. We recommend that this initial calibration step can be taken with $\tau_{\gamma} = 0$ (i.e., no piecewise linear cost). Then, the value of τ_{γ} can be fine-tuned to better balance deviations of sampling probabilities across segments. Our experience suggests that values for τ_{γ} between 0 and 0.4 provide adequate results.

References

- Abatzoglou, J.T., Brown, T.J., 2012. A comparison of statistical downscaling methods suited for wildfire applications. Int. J. Climatol. 32 (5), 772–780. https://doi.org/ 10.1002/joc.2312.
- Allan, R.P., Barlow, M., Byrne, M.P., Cherchi, A., Douville, H., Fowler, H.J., Gan, T.Y., Pendergrass, A.G., Rosenfeld, D., Swann, A.L.S., Wilcox, L.J., Zolina, O., 2020.
 Advances in understanding large-scale responses of the water cycle to climate change. *Ann. N.Y.* Acad. Sci. 1472. 49–75. https://doi.org/10.1111/nvas.14337.
- Berg, N., Hall, A., 2017. Anthropogenic warming impacts on California snowpack during drought. Geophys. Res. Lett. 44, 2511–2518. https://doi.org/10.1002/ 2016GL072104.
- Brown, C., Ghile, Y., Laverty, M., Li, K., 2012. Decision scaling: Linking bottom-up vulnerability analysis with climate projections in the water sector. Water Resour. Res. 48. W09537. https://doi.org/10.1029/2011WR011212.
- CA-DWR CCTAG (2015), Perspectives and guidance for climate change analysis, Technical Report, August 2015. https://water.ca.gov/-/media/DWR-Website/Web-Pages/Programs/All-Programs/Climate-Change-Program/Climate-Program-Activities/Files/Reports/Perspectives-Guidance-Climate-Change-Analysis.pdf.
- Dettinger, M., 2016. Historical and Future Relations Between Large Storms and Droughts in California. San Francisco Estuary and Watershed Science 14 (2). https://doi.org/1 0.15447/sfews.2016v14iss2art1.
- CA DWR (2019), Decision Scaling Evaluation of Climate Change Driven Hydrologic Risk to the State Water Project, Technical Report, May 2019. https://water.ca.gov/-/media/DWR-Website/Web-Pages/Programs/All-Programs/Climate-Change-Program/Climate-Action-Plan/Files/CAP-III-Decision-Scaling-Vulnerability-Assessment.pdf.
- Elbaum, E., Garfinkel, C.I., Adam, O., Morin, E., Rostkier-Edelstein, D., Dayan, U., 2022. Uncertainty in projected changes in precipitation minus evaporation: Dominant role of dynamic circulation changes and weak role for thermodynamic changes. e2022GL097725 Geophys. Res. Lett. 49. https://doi.org/10.1029/2022GL097725.
- Espinoza, V., Waliser, D.E., Guan, B., Lavers, D.A., Ralph, F.M., 2018. Global analysis of climate change projection effects on atmospheric rivers. Geophys. Res. Lett. 45, 4299–4308. https://doi.org/10.1029/2017GL076968.
- Gao, Y., Lu, J., Leung, L.R., 2016. Uncertainties in projecting future changes in atmospheric rivers and their impacts on heavy precipitation over Europe. J. Clim. 29, 6711–6726.
- Gershunov, A., Shulgina, T., Clemesha, R.E.S., et al., 2019. Precipitation regime change in Western North America: The role of Atmospheric Rivers. Sci. Rep. 9, 9944. https://doi.org/10.1038/s41598-019-46169-w.
- Gonzales, K.R., Swain, D.L., Nardi, K.M., Barnes, E.A., Diffenbaugh, N.S., 2019. Recent warming of landfalling atmospheric rivers along the west coast of the United States. J. Geophys. Res. Atmos. 24, 6810–6826.
- Gu, L., Yin, J., Gentine, P., Wang, H., Slater, L.J., Sullivan, S.C., Chen, J., Zscheischler, J., Guo, S., 2023. Large anomalies in future extreme precipitation sensitivity driven by atmospheric dynamics. Nat. Commun. 14 (1), 1–13. https://doi.org/10.1038/s41467-023-39039-7.
- Hayhoe, K., Stoner, A., Wuebbles, D.J., et al. (2023). STAR-ESDM: A Generalizable Approach to Generating High-Resolution Climate Projections through Signal Decomposition. ESS Open Archive. September 13, 2023. DOI: 10.22541/ essoar.169462036.65393270/v1.
- He, M., Anderson, J., Lynn, E., Arnold, W., 2021. Projected Changes in Water Year Types and Hydrological Drought in California's Central Valley in the 21st Century. Climate 9 (2), 26. https://doi.org/10.3390/cli9020026.
- Huang, X., Swain, D.L., 2022. Climate change is increasing the risk of a California megaflood. Science. Advances 8 (31). https://doi.org/10.1126/sciadv.abq0995.
- IPCC (2022). Climate Change 2022: Impacts, Adaptation, and Vulnerability.
 Contribution of Working Group II to the Sixth Assessment Report of the Intergovernmental Panel on Climate Change [H.-O. Pörtner, D.C. Roberts, M. Tignor, E.S. Poloczanska, K. Mintenbeck, A. Alegría, M. Craig, S. Langsdorf, S. Löschke, V. Möller, A. Okem, B. Rama (eds.)]. Cambridge University Press. Cambridge University Press, Cambridge, UK and New York, NY, USA, 3056 pp., doi:10.1017/9781000325844
- Ishida, K., Ohara, N., Ali Ercan, S., Jang, T., Trinh, M.L., Kavvas, K.C., Anderson, M.L., 2019. Impacts of climate change on snow accumulation and melting processes over mountainous regions in Northern California during the 21st century. Sci. Total Environ. 685, 104–115.
- Kuo, N., Kim, H., Lehner, F., 2023. Anthropogenic Aerosols Contribute to the Recent Decline in Precipitation Over the U.S. e2023GL105389 Southwest. *Geophysical Research Letters* 50 (23). https://doi.org/10.1029/2023GL105389.
- Livneh, B., Rosenberg, E.A., Lin, C., Nijssen, B., Mishra, V., Andreadis, K.M., Maurer, E. P., Lettenmaier, D.P., 2013. A long-term hydrologically based dataset of land surface fluxes and states for the conterminous United States: Update and extensions.
 J. Climate 26, 9384–9392. https://doi.org/10.1175/JCLI-D-12-00508.1.
- Ma, W., Chen, G., Guan, B., 2020. Poleward shift of atmospheric rivers in the Southern Hemisphere in recent decades. Geophys. Res. Lett. 47 (21) e2020GL089934.

- Massoud, E.C., Espinoza, V., Guan, B., Waliser, D.E., 2019. Global Climate Model Ensemble Approaches for Future Projections of Atmospheric Rivers. Earth's Future 7, 1136–11511151. https://doi.org/10.1029/2019EF001249.
- Michaelis, A.C., Gershunov, A., Weyant, A., Fish, M.A., Shulgina, T., Ralph, F.M., 2022. Atmospheric river precipitation enhanced by climate change: A case study of the storm that contributed to California's Oroville Dam crisis. Earth's. e2021EF002537 Future 10. https://doi.org/10.1029/2021EF002537.
- Najibi, N., Steinschneider, S., 2023. Extreme precipitation-temperature scaling in California: The role of Atmospheric Rivers. e2023GL104606 Geophys. Res. Lett. 50 (14). https://doi.org/10.1029/2023GL104606.
- Overpeck, J.T., Udall, B., 2020. Climate change and the aridification of North America, *The.* Proc. Natl. Acad. Sci. 117 (22), 11856–11858.
- Payne, A.E., Demory, M.E., Leung, L.R., et al., 2020. Responses and impacts of atmospheric rivers to climate change. Nat Rev Earth Environ 1, 143–157. https://doi.org/10.1038/s43017-020-0030-5.
- Pendergrass, A.G., Hartmann, D.L., 2014. The atmospheric energy constraint on global-mean precipitation change. J. Clim. 27 (2), 757–768.
- Pfahl, S., O'Gorman, P.A., Fischer, E.M., 2017. Understanding the regional pattern of projected future changes in extreme precipitation. Nat. Clim. Chang. 7 (6), 423–427.
- Pierce, D.W., Su, L., Cayan, D.R., Risser, M.D., Livneh, B., Lettenmaier, D.P., 2021. An extreme-preserving long-term gridded daily precipitation dataset for the conterminous United States. J. Hydrometeorol. 22 (7), 1883–1895.
- Pierce, D.W., Cayan, D.R., Feldman, D.R., Risser, M.D., 2023. Future Increases in North American Extreme Precipitation in CMIP6 Downscaled with LOCA. J. Hydrometeor. 24, 951–975. https://doi.org/10.1175/JHM-D-22-0194.1.
- PRISM Climate Group, 2014, Oregon State University, https://prism.oregonstate.edu, data created 4 Feb 2014.
- Ranasinghe, R., A.C. Ruane, R. Vautard, N. Arnell, E. Coppola, F.A. Cruz, S. Dessai, A.S. Islam, M. Rahimi, D. Ruiz Carrascal, J. Sillmann, M.B. Sylla, C. Tebaldi, W. Wang, and R. Zaaboul (2021). Climate Change Information for Regional Impact and for Risk Assessment. In Climate Change 2021: The Physical Science Basis. Contribution of Working Group I to the Sixth Assessment Report of the Intergovernmental Panel on Climate Change [Masson-Delmotte, V., P. Zhai, A. Pirani, S.L. Connors, C. Péan, S. Berger, N. Caud, Y. Chen, L. Goldfarb, M.I. Gomis, M. Huang, K. Leitzell, E. Lonnoy, J.B.R. Matthews, T.K. Maycock, T. Waterfield, O. Yelekçi, R. Yu, and B. Zhou (eds.)]. Cambridge University Press, Cambridge, United Kingdom and New York, NY, USA, pp. 1767–1926, doi: 10.1017/9781009157896.014.
- Ray, P., Wi, S., Schwarz, A., Correa, M., He, M., Brown, C., 2020. Vulnerability and risk: Climate change and water supply from California's Central Valley water system. Clim. Change 161, 177–199.
- Rhoades, A.M., Jones, A.D., Srivastava, A., Huang, H., O'Brien, T.A., Patricola, C.M., Zhou, Y., 2020. The shifting scales of western US landfalling atmospheric rivers under climate change. Geophys. Res. Lett. 47 (17) e2020GL089096.
- Robertson, A.W., Y. Kushnir, U. Lall, and J. Nakamura (2015), Weather and climatic drivers of extreme flooding events over the Midwest of the United States. Extreme Events: Observations, Modeling, and Economics, *Geophys. Monogr.*, 214, Amer. Geophys. Union, 113–124.
- Robertson, A.W., Ghil, M., 1999. Large-scale weather regimes and local climate over the western United States. J. Clim. 12, 1796–1813.
- Schwarz, A., Ray, P., Wi, S., Brown, C., He, M., & Correa, M. (2018). Climate change risks faced by the California Central Valley water resource system. California's fourth climate change assessment. Publication number: CCCA4-EXT-2018-001. https://www. energy.ca.gov/sites/default/files/2019-12/Water CCCA4-EXT-2018-001 ada.pdf.
- Shepherd, T., 2014. Atmospheric circulation as a source of uncertainty in climate change projections. Nature Geosci. 7, 703–708. https://doi.org/10.1038/ngeo2253.
- Shields, C.A., Kiehl, J.T., 2016. Atmospheric river landfall-latitude changes in future climate simulations. Geophys. Res. Lett. 43, 8775–8782.
- Shulgina, T., Gershunov, A., Hatchett, B. J., Guirguis, K., Subramanian, A. C., Margulis, Fang, Y., Cayan, D.R., Pierce, D.W., Dettinger, M., Anderson, M.L., & Ralph, F. M. (2023). Observed and projected changes in snow accumulation and snowline in California's snowy mountains. Climate Dynamics, 1-16.
- Steinschneider, S., McCrary, R., Wi, S., Mulligan, K., Mearns, L., Brown, C., 2015. Expanded Decision-Scaling Framework to Select Robust Long-Term Water-System Plans under Hydroclimatic Uncertainties. J. Water Resour. Plann. Manage. 141 (11), 04015023. https://doi.org/10.1061/CASCEJWR.1943-5452.0000536.
- Swain, D.L., Langenbrunner, B., Neelin, J.D., Hall, A., 2018. Increasing precipitation volatility in twenty-first-century California. Nat. Clim. Chang. 8 (5), 427–433.
- Ullrich, P.A., Xu, Z., Rhoades, A.M., Dettinger, M.D., Mount, J.F., Jones, A.D., Vahmani, P., 2018. California's drought of the future: A midcentury recreation of the exceptional conditions of 2012–2017. Earth's Future 6, 1568–1587.
- Williams, A.P., Cook, B.I., Smerdon, J.E., 2022. Rapid intensification of the emerging southwestern North American megadrought in 2020–2021. Nat. Clim. Chang. 12, 232–234.
- Zhang, W., Hari, V., S-Y Wang, S., LaPlante, M. D., Garfin, G., Affram, G., & Kumar, R. (2022). Fewer troughs, not more ridges, have led to a drying trend in the western United States. Geophysical Research Letters, 49, e2021GL0.